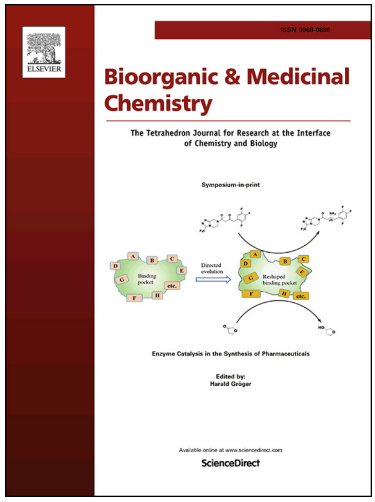

Discovery of novel 2,5-dihydroxyterephthalamide derivatives as multifunctional agents for the treatment of Alzheimer's disease

Qing Song, Yan Li, Zhongcheng Cao, Hongyan Liu, Chaoquan Tian, Ziyi Yang, Xiaoming Qiang, Zhenghuai Tan, Yong Deng

PII: S0968-0896(18)31761-9
DOI: https://doi.org/10.1016/j.bmc.2018.11.015
Reference: BMC 14619

To appear in: *Bioorganic & Medicinal Chemistry*

Received Date: 15 October 2018
Revised Date: 10 November 2018
Accepted Date: 12 November 2018

Please cite this article as: Song, Q., Li, Y., Cao, Z., Liu, H., Tian, C., Yang, Z., Qiang, X., Tan, Z., Deng, Y., Discovery of novel 2,5-dihydroxyterephthalamide derivatives as multifunctional agents for the treatment of Alzheimer's disease, *Bioorganic & Medicinal Chemistry* (2018), doi: https://doi.org/10.1016/j.bmc.2018.11.015

Discovery of novel 2,5-dihydroxyterephthalamide derivatives as multifunctional agents for the treatment of Alzheimer's disease

Qing Song[a], Yan Li[a], Zhongcheng Cao[a], Hongyan Liu[a], Chaoquan Tian[a], Ziyi Yang[a], Xiaoming Qiang[a], Zhenghuai Tan[b], Yong Deng[a,*]

[a]*Department of Medicinal Chemistry, Key Laboratory of Drug-Targeting and Drug Delivery System of the Education Ministry, Sichuan Engineering Laboratory for Plant-Sourced Drug and Sichuan Research Center for Drug Precision Industrial Technology, West China School of Pharmacy, Sichuan University, Chengdu, 610041, P. R. China*

[b]*Institute of Traditional Chinese Medicine Pharmacology and Toxicology, Sichuan academy of Chinese Medicine Sciences, Chengdu, 610041, P. R. China*

**Corresponding Author*.

E-mail: dengyong@scu.edu.cn (Yong Deng)

Abstract

A series of 2,5-dihydroxyterephthalamide derivatives were designed, synthesized and evaluated as multifunctional agents for the treatment of Alzheimer's disease. *In vitro* assays demonstrated that most of the derivatives exhibited good multifunctional activities. Among them, compound **9d** showed the best inhibitory activity against both *Rat*AChE and *Ee*AChE (IC_{50} = 0.56 μM and 5.12 μM, respectively). Moreover, **9d** exhibited excellent inhibitory effects on self-induced Aβ_{1-42} aggregation (IC_{50} = 3.05 μM) and Cu^{2+}-induced Aβ_{1-42} aggregation (71.7% at 25.0 μM), and displayed significant disaggregation ability to self- and Cu^{2+}-induced Aβ_{1-42} aggregation fibrils (75.2% and 77.2% at 25.0 μM, respectively). Furthermore, **9d** also showed biometal chelating abilities, antioxidant activity, anti-neuroinflammatory activities and appropriate BBB permeability. These multifunctional properties highlight **9d** as promising candidate for further studies directed to the development of novel drugs against AD.

Keywords:

Alzheimer's disease; 2,5-Dihydroxyterephthalamide derivatives; Acetylcholinesterase inhibitors; Aβ aggregation inhibitors; Antioxidant; Anti-neuroinflammatory agents

1. Introduction

Alzheimer's disease (AD) is a progressive neurodegenerative disorder characterized by memory loss and cognitive impairments, which can cause both physical and mental injury even resulting in death.[1,2] According to the World Alzheimer Report, there were 46.8 million people worldwide suffering from dementia in 2015 and this number will reach 131.5 million in 2050.[3] AD has multifactorial pathophysiological hallmarks.[4] Although the exact etiology of AD remains unknown, many factors have been described to play definitive roles in its pathogenesis, including degeneration of cholinergic neurons, β-amyloid (Aβ) deposition, τ-protein aggregation, dyshomeostasis of biometals, oxidative stress, and neuroinflammation.[5]

"Cholinergic hypothesis" of AD demonstrated there was a functional impairment of basal forebrain cholinergic neurons with the consequence of the decreased levels of acetylcholine (ACh) resulting in learning and memory dysfunctioning.[6] Following this, Acetylcholinesterase (AChE) was validated as a therapeutic target to increase cholinergic levels, and AChE inhibitors are effective in temporarily restoring cholinergic function. Recently, AChE was indicated to be involved in Aβ aggregation-promoting action. Bivalent AChE inhibitors simultaneously blocking both the catalytic active site (CAS) and particularly the peripheral anionic sites (PAS) might not only alleviate the cognitive deficit of AD patients by elevating ACh levels, but also act as disease-modifying agents delaying amyloid plaque formation.[7] Butyrylcholinesterase (BuChE) is also the key enzyme that plays important roles in cholinergic transmission by hydrolyzing the neurotransmitter ACh. However, serious inhibition of BuChE may contribute to the potential peripheral side effects of ChE inhibitors, for instance tacrine, the dual AChE and BuChE inhibitor, has shown severe hepatotoxicity and many other adverse effects.[8]

"Amyloid hypothesis" indicates that the abnormal production and accumulation of Aβ forms insoluble amyloid fibrils, which can deposit in senile plaques in the critical regions of brain.[9] There are two major forms of Aβ peptides. A$\beta_{1\text{-}40}$, the dominant one, is soluble and less neurotoxic. Another one is A$\beta_{1\text{-}42}$ peptide, which constitutes 5-10% in normal conditions. It is considered to be aberrant in AD brains and can result in larger oligomers and fibrils.[10] So counteracting brain damage by inhibiting the A$\beta_{1\text{-}42}$ aggregation or promoting its depolymerization can be a potent treatment for AD.

Increasing evidence suggests that Aβ plaques directly interfere with the electron transfer chain

and produce free radicals, resulting in oxidative stress.[11] Due to high reactivity, some of these superoxide free radicals can react with nitrate, leading to the formation of highly reactive oxygenation of the nitrous oxide free radicals.[12] On the other hand, the increase of production of reactive oxygen species (ROS) and free radicals leads to deleterious effects on the cell components, and it's accepted as central processes in AD pathophysiology.[13] What's more, the process of cellular oxidation is linked to the oxidation reduction of certain metals. The changes of ion concentration can cause oxidative stress and increase the production of ROS. Cu^{2+}, Zn^{2+} and other metals can also influence the processes of protein aggregation. Amyloid precursor protein (APP) and Aβ are able to form complexes with these biometals, which can promote the aggregation of Aβ.[14] According to these, molecules with antioxidant and metal-chelating abilities may be a good therapy for AD.

With the emphasis on the inflammatory mechanism of AD in recent years, it's proposed that neuroinflammation may be another important pathogenesis of AD.[15] Neuroinflammation of AD is mainly manifested by activation of microglia cells. Under normal physiological conditions, microglia cells are resting.[16] However, in neurodegenerative diseases, microglia cells are constantly activated and release a variety of inflammatory cytokines leading to chronic neuroinflammation. Studies showed these inflammatory cytokines could also aggravate oxidative stress in the brain and further stimulate the generation, aggregation and deposition of Aβ. Other studies have shown that activation of microglia occurs before neurodegenerative symptoms appear, and may be an early event of pathological changes in AD.[17,18] Thus, anti-neuroinflammatory agents are considered potential candidates for anti-Alzheimer drugs.

Epidemiological studies suggest that nonsteroidal anti-inflammatory drugs (NSAIDs) can significantly reduce the incidence of AD. Researches showed NSAIDs could even control the release of inflammatory factors and oxygen free radicals caused by the deposition of Aβ, and reduce the amount and area of Aβ deposition.[19,20] Salicylic acid (**Figure 1a**) is a classic NSAID with a long history of medicication. Besides the anti-inflammatory activity, salicylic acid has been extensively studied for the antioxidative and metal-chelating properties.[21,22] It even has certain anticholinesterase activity (IC_{50} = 346.0 μM).[23] These researches show that salicylic acid and its derivatives can be used against multiple targets in AD disease, suggesting that they can be used as a precursor drug to design new anti-AD chemicals.

Due to the complex etiology of AD, the single-target directed drugs that have reached clinical

trials have failed. Recently, more researches in AD have been paid attention to the development of ‘‘multi-target-directed ligands’’ (MTDLs), by which new scaffolds aiming at two or more diseases targets are designed. Based on previous research of our group, the introduction of the alkylbenzylamine group to genistein significantly increased the inhibitory activity of AChE, and the modified genistein derivatives are multifunctional for AD treatment.[24] In addition, inspired by the multitarget anti-AD compound Memoquin (**Figure 1b**) reported by Melchiorre's group,[25] bialkaline central modification can significantly enhance the activity of compounds. Therefore, we designed a series of 2,5-dihydroxyterephthalamide (DHTA) derivatives (**Figure 1c**) by combining 2,5-dihydroxyterephthalic acid with appropriate secondary amines using carbon spacers of different lengths, and evaluated for their multifunctional biological activities about effects on Aβ aggregation and disaggregation, anti-inflammatory activity, AChE inhibition activity, anti-oxidative and metal chelating properties.

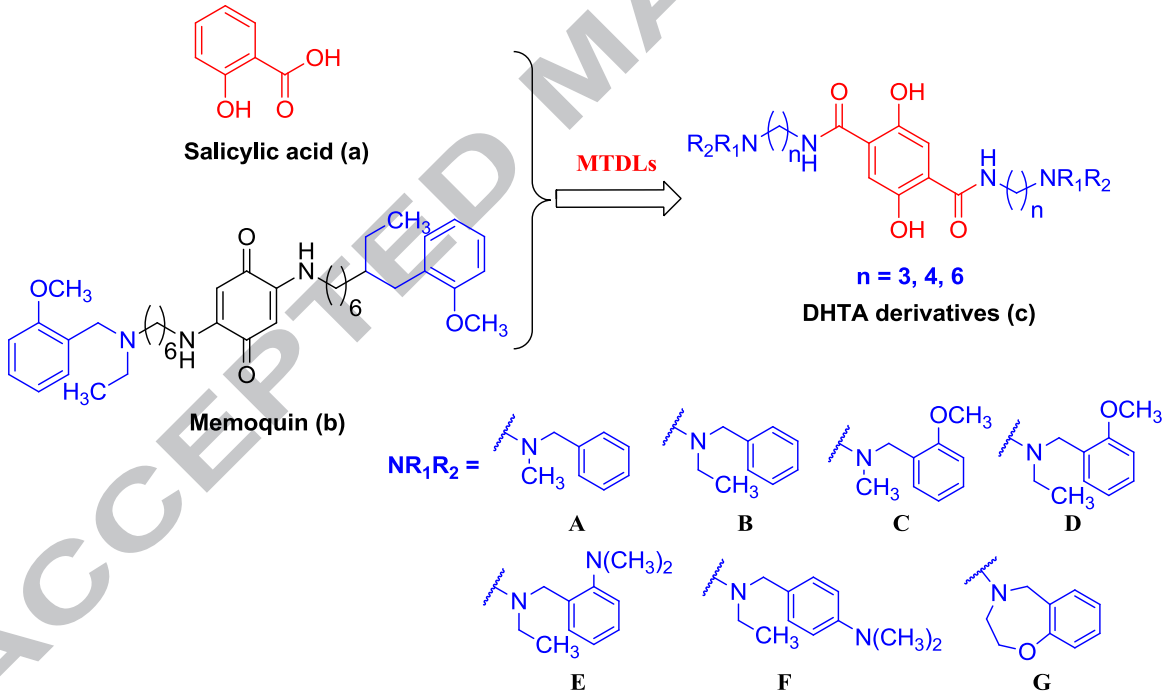

Figure 1. Design strategy followed for the development of multifunctional DHTA derivatives.

2. Results and discussion

2.1 Chemistry

The synthetic pathways of target derivatives were summarized in **Scheme 1**. Compound **2** was synthesized from diethyl succinate (**1**) by Claisen-Dieckmann condensation under the condition of

sodium ethanol/ethanol.[26] Then, in the presence of *N*-chlorosuccinimide, compound **3** was obtained through aromatization reaction.[27] It was hydrolyzed under alkaline conditions to get the key intermediate **4**. Compound **4** was condensed with the corresponding primary amine **5-7**[28] in the presence of 1-(3-dimethylaminopropyl)-3-ethyl carbon imine hydrochloride (EDCI) and 1-hydroxybenzotriazole (HOBt) in THF to provide the DHTA derivatives **8-10**.[29] All of the target compounds were characterized by ^{1}H NMR and ESI-MS, and most of them were further characterized by ^{13}C NMR. The purity of all target compounds was determined by high-performance liquid chromatography (HPLC) analysis to be over 96.5 %.

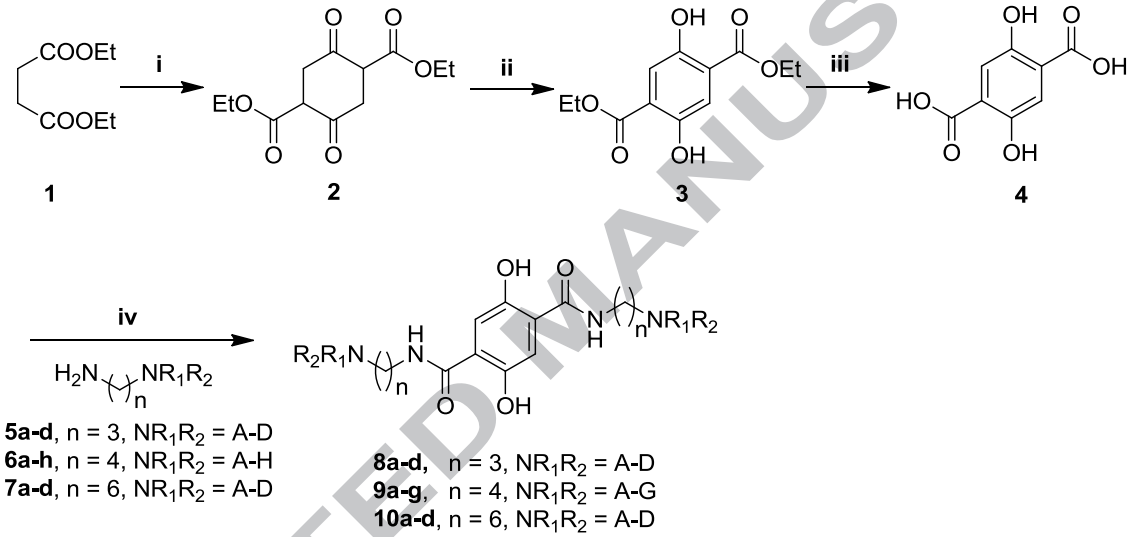

Scheme 1. Synthesis of DHTA derivatives **8-10**. *Reagents and conditions:* (i) NaOEt, EtOH, reflux, 5 h; then 1.0 mol/L H_2SO_4, r.t., 5 h; (ii) *N*-Chlorosuccinimide, HOAc, 80 °C, 5 h; (iii) NaOH, H_2O, 80 °C, argon atmosphere, 5 h; then *conc*. HCl; (iv) corresponding amine **5~7**, EDCI, HOBt, Et_3N, THF, r.t., overnight.

2.2 Biological evaluation

2.2.1 Evaluation of AChE and BuChE inhibitory activities of DHTA derivatives

The inhibitory activities of all the synthesized DHTA derivatives against AChE and BuChE *in vitro* were evaluated according to modified Ellman's method.[24,30] AChE inhibitory activity was measured from both rat cortex homogenate and *Electrophorus electricus*, and BuChE inbibitory activity was measured from rat serum. Donepezil and rivastigmine were used as reference compounds. The ChE inhibitory results are summarized in **Table 1**.

Most of the tested compounds showed moderate AChE inhibitory activities with IC_{50} values

ranging from submicromolar to micromolar (0.56-30.80 μM), which were better than that of rivastigmine. Comparing the activities of compound **4** with DHTA derivatives, it could be found that the introduction of the alkylbenzylamine group could significantly increase the AChE inhibitory activities as expected. Further structure-activity relationship analysis showed that the length of methylene side chain and the type of terminal benzyl amine also had important effects on the activity. The four methylene length side chain compounds (**9a-d**, IC_{50} = 0.56-7.37 μM) had higher activity than the corresponding three and six methylene length compounds (**8a-d**, IC_{50} = 0.67-11.30 μM; **10a-d**, IC_{50} = 1.68-10.60 μM). Therefore, a four-methylene linker was beneficial for AChE inhibitory activity. Fixing the side chain length, it could be found that compounds with (2-methoxy benzyl) ethylamine moieties (**8d**, **9d** and **10d**) had higher activity, indicating that (2-methoxy benzyl) ethylamine moiety is the best substitute group. And the introduction of (4-dimethylamine benzyl) ethylamine and 2,3,4,5-tetrahydrobenzo[*f*][1,4]oxazepine heterocyclic moieties (**9f** and **9g**) significantly decreased the activity. Among the tested derivatives, compound **9d** exhibited the most potent inhibitory activity aginst both *Rat*AChE and *Ee*AChE (IC_{50} = 0.56 ± 0.022 μM and 5.12 ± 0.16 μM, respectively), which was more excellent than rivastigmine (IC_{50} = 37.10 ± 1.22 μM and 23.20 ± 0.44 μM, respectively) under our experimental condition. But **9d** had relatively poor activity than Memoquin (IC_{50} = 1.55 ± 0.11 nM) [25] although it possessed almost the same substitute group, the reason may lie in the difference of the mother nucleus.

In addition, most DHTA derivatives were inactive or weak on BuChE inhibitory activity. This result showed that the designed target compounds were potent inhibitors with high selectivity toward AChE. Compound **8c**, **9c** and **10c** had relatively good BuChE inhibitory activity with IC_{50} values of 17.30 ± 0.33 μM, 19.20 ± 0.65 μM and 40.50 ± 0.56 μM, respectively, indicating that (2-methoxy benzyl) methylamine moiety may be favorable for the contacts with BuChE.

Table 1. *In vitro* inhibition of AChE and BuChE and Oxygen Radical Absorbance Capacity (ORAC, Trolox Equivalents) by DHTA derivatives and reference compounds.

Compd.	n	NR_1R_2	IC_{50} (μM) ± SD[a]			ORAC[e]
			*Rat*AChE[b]	*Rat*BuChE[c]	*Ee*AChE[d]	
3	—	—	> 100	> 100	> 100	0.96 ± 0.02
4	—	—	> 100	> 100	> 100	4.70 ± 0.10

8a	3		11.30 ± 0.20	> 100	14.10 ± 0.17	1.21 ± 0.05
8b	3		7.80 ± 0.19	> 100	26.80 ± 0.75	0.95 ± 0.01
8c	3	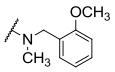	9.21 ± 0.37	17.30 ± 0.33	39.70 ± 0.63	1.37 ± 0.06
8d	3	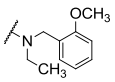	0.67 ± 0.013	> 100	11.40 ± 0.27	1.10 ± 0.04
9a	4	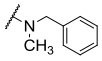	5.21 ± 0.18	> 100	12.60 ± 0.22	1.52 ± 0.06
9b	4	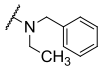	4.05 ± 0.18	> 100	14.00 ± 0.33	0.93 ± 0.02
9c	4	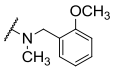	7.37 ± 0.23	19.2 ± 0.65	5.87 ± 0.11	0.64 ± 0.01
9d	4	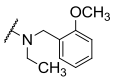	0.56 ± 0.023	> 100	5.12 ± 0.16	0.97 ± 0.05
9e	4	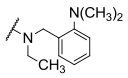	4.17 ± 0.16	> 100	10.80 ± 0.13	1.16 ± 0.03
9f	4	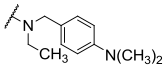	27.40 ± 0.83	> 100	47.40 ± 0.17	3.23 ± 0.07
9g	4		30.80 ± 1.11	> 100	64.80 ± 3.01	1.02 ± 0.01
10a	6	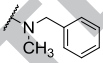	5.60 ± 0.17	41.9 ± 1.05	13.10 ± 0.28	1.01 ± 0.02
10b	6	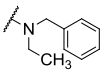	4.60 ± 0.12	47.2 ± 0.73	22.90 ± 0.70	1.27 ± 0.06
10c	6	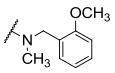	10.60 ± 0.56	40.5 ± 0.56	6.11 ± 0.11	0.62 ± 0.02
10d	6	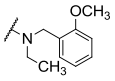	1.68 ± 0.04	> 100	6.75 ± 0.17	1.43 ± 0.03
Rivastigmine	—	—	37.10 ± 1.22	9.87 ± 0.23	23.20 ± 0.44	n.t.[g]
Donepezil	—	—	0.015 ± 0.002	20.70 ± 0.36	0.021 ± 0.003	n.t.[g]

[a] IC_{50} values represent the concentration of inhibitor required to decrease enzyme activity by 50% and are the mean of three independent experiments, each performed in triplicate (SD = standard deviation).

[b] From 5% rat cortex homogenate.

[c] From rat serum.

[d] From *Electrophorus electricus*.

[e] The mean ± SD of the three independent experiments. The data are expressed as μM of Trolox equiv/μM of tested compound.

[f] n.a. = no active. Compounds defined "no active" means that percent inhibition is less than 5.0% at a concentration of 50 μM in the assay conditions.

[g] n.t. = not tested.

2.2.2 Evaluation of AChE inhibition mechanism

To further understand the inhibitory mechanism of DHTA derivatives, compound **9d**, the most potent AChE inhibitor among these compounds, was chosen for a kinetic study using *Ee*AChE.[31] From the illustration of the reciprocal Lineweaver-Burk plots (**Figure 2**), it could be seen that as the concentration of **9d** increased, both the slopes (decreased V_{max}) and intercepts (higher K_m) increased. This pattern indicated a mixed-type inhibitory behavior for **9d** as the consequence of binding to both the CAS and PAS of AChE.

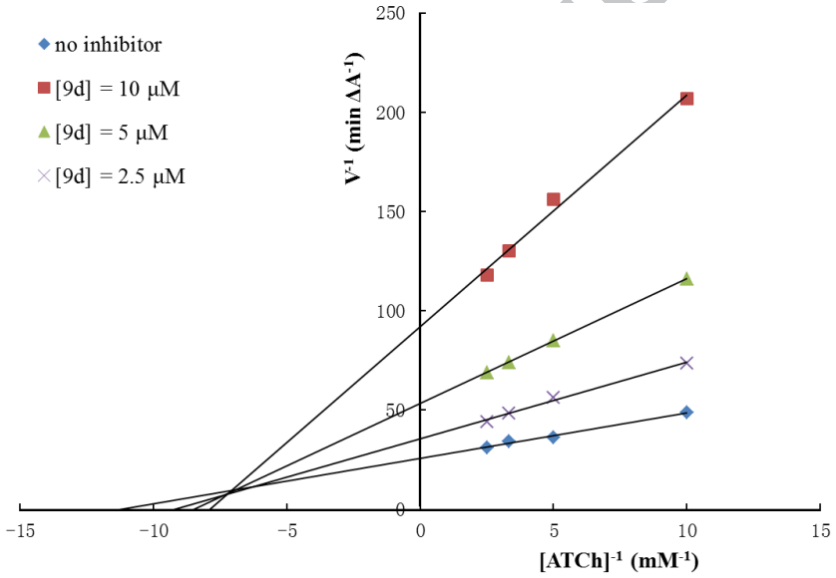

Figure 2. Kinetic study on the mechanism of *Ee*AChE inhibition by compound **9d**. In the absence and presence of **9d**, overlapping Lineweaver-Burk reciprocal plots of the initial velocity of AChE at increasing substrate concentration (0.1-0.4 mM) are shown. Lines were derived from a weighted least-squares analysis of data points.

2.2.3 Molecular modeling studies

To explore the possible interaction pattern between DHAT derivatives and *Torpedo californica (Tc)*AChE (PDB code: *1EVE*), a molecular modeling research was conducted using the docking program, AutoDock 4.2 package with Discovery Studio 2.5.[32] Compound **9d** was selected for our molecular modeling studies after comprehensive consideration of the results of AChE inhibition assay and kinetic study. As the results shown in **Figure 3**, compound **9d** occupied the entire

enzymatic CAS, the mid-gorge sites and the PAS, while simultaneously binding to the catalytic site and peripheral site. In the *Tc*AChE-**9d** complex, the phenolic hydroxyl groups and the carbonyl groups of amide in **9d** could form intermolecular hydrogen bond with the carbonyl group of amino acid residues Asp72 and the hydroxyl group of Try121 respectively (**9d**-OH• • •O=Asp72; **9d**=O• • •OH-Tyr121). The *N*-(2-methoxybenzyl) ethylamine moiety interacted with Trp84 on the CAS *via* parallel π-π interactions. It also had a potential hydrophobic interaction with Gly117, Gly118, Gly123, Tyr130, and Glu199. And the amide fragment and the benzene ring at the center of the molecule could also interact with Phe331 and Tyr334 respectively *via* a certain parallel π-π interaction. In addition, the molecular folded conformation of **9d** induced a hydrophobic interaction with residues such as Tyr70, Ser81, Trp279, Leu282, Ser286, Ile287, Phe288, Arg289, Phe290, Phe330 and His440 in the active sites of enzymes. In conclusion, the results of enzyme kinetics studies and molecular docking studies are consistent, indicating that compound **9d** can simultaneously binding to the CAS and PAS parts of AChE, which explains the moderate AChE inhibition activity of DHTA derivatives.

Studies showed that the amino acid sequences and crystal structures were different between *Ee*AChE and *Rat*AChE.[33] So there may be different binding site between compounds with acetylcholinesterase from different sources. To further elucidate why the IC_{50} value of **9d** against *Ee*AChE (IC_{50} = 5.12 μM) is much higher than that against *Rat*AChE (IC_{50} = 0.56 μM), docking studies of **9b** with mouse AChE (mAChE, PDB code: 4B85) was also performed (**Figure S2**, Supplementary Material). The results showed, in the mAChE-**9d** complex, the two phenolic hydroxyl groups in **9d** could respectively form intermolecular hydrogen bond with the carbonyl group of amino acid residues Tyr124 and the hydroxyl group of Phe295 (**9d**-OH• • •O=Tyr124; **9d**-O• • •OH-Phe295). The carbonyl groups of amide in **9d** could form intermolecular hydrogen bond with the hydroxyl groups of Arg296 and Phe295 (**9d**=O• • •OH- Arg296; **9d=O• • •OH-** Phe295). In addition, the *N*-(2-methoxybenzyl) ethylamine moiety interacted with Trp86 *via* parallel π-π interactions, and the salicylic acid nucleus could also interact with Tyr341 *via* parallel π-π interactions. Compared with *Tc*AChE-**9d** complex, there were more intermolecular hydrogen bonds in the mAChE-**9d** complex, which may give the reason of the higher activity of **9d** against *Rat*AChE than that against *Ee*AChE.

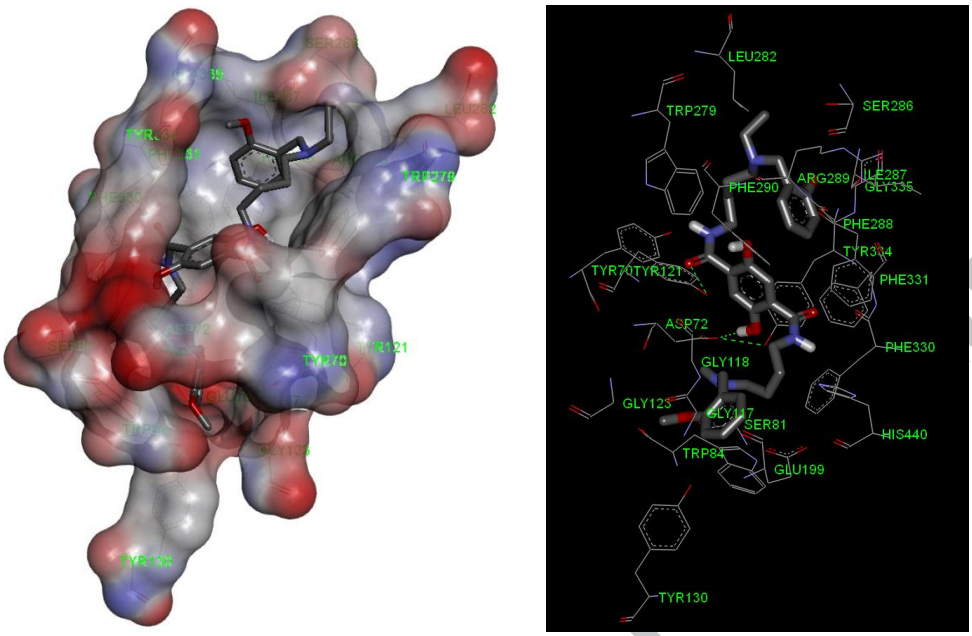

Figure 3. Representation of compound **9d** (grey stick) interacting with residues in the binding site of *Tc*AChE (PDB code: *1EVE*), highlighting the protein residues involved in the major interactions with the inhibitor. Picture was generated using Discovery Studio 2.5.

2.2.4 Antioxidant activity assay of DHTA derivatives

The antioxidant activities of DHTA derivatives were evaluated by the well-established ORAC-FL method (oxygen radical absorbance capacity by fluorescein)[34] and the results are shown in **Table 1**. The activities of tested compounds to scavenge radicals were expressed as Trolox (a water-soluble vitamin E analog) equivalent. And their relative activity at concentration of 5 μM was compared with the highly potent compound Trolox. All of the compounds exhibited significant antioxidant activities ranging from 0.62 to 3.23-fold of Trolox. And the parent compounds **3** and **4** were also tested, which had ORAC-FL values of 0.96 and 4.70 Trolox equivalents, respectively, Most of the derivatives had similar antioxidant activities to compound **3** due to the amidation of carboxyl groups. Compared with the lead compound Memoquin (0.77 Trolox equivalents) [25], most of the derivatives had better antioxidant activities than it. There was no significant effect on the activity of other tertiary amine species and the side chain length. Among them, compound **9f** showed the most potent antioxidant activity of this family with ORAC-FL values of 3.23 Trolox equivalents. Representative compound **9d** showed good antioxidant activity with an ORAC-FL value of 0.97 Trolox equivalent.

2.2.5 Metal-chelating studies of representative compound 9d

The chelating abilities of representative compound **9d** toward biometals such as Cu^{2+}, Zn^{2+}, Fe^{2+} and Al^{3+} were evaluated by UV-visual spectrometry,[35,36] and the results are shown in **Figure 4**. It could be seen that, after the addition of $CuCl_2$, the UV-visual spectrum of **9d** changed significantly. The absorption peak at the original 260 nm shifted to 274 nm with the absorption intensity increasing significantly, and the absorption peak at 360 nm disappeared, indicating that compound **9d** had a certain chelating effect on Cu^{2+}. After the addition of $AlCl_3$, the absorption intensity at 260 nm was increased, and the absorption peak at the original 360 nm was moved to 351 nm, indicating the interaction between compound **9d** with Al^{3+}. In addition, after adding $FeSO_4$ to the solution of **9d**, the UV-Visual spectrum significantly changed and the absorption intensity increased dramatically, indicating **9d** and Fe^{2+} had certain interaction. However, there was no significant change in the spectrum after $ZnCl_2$ was added. These results showed that **9d** had the ability to interact with most biometals.

To determine the stoichiometry of **9d**-Cu^{2+} complex, molar ratio method was performed by preparing the methanol solution of **9d** with ascending amounts of $CuCl_2$. The UV spectra were used to obtain the absorbance of the **9d** complexes and different concentrations of $CuCl_2$ at 274 nm. As indicated in **Figure 4B**, the absorbance linearly increased initially and then plateaued. The point for the straight lines to intersect were determined to be at a mole proportion of 1.90, revealing 1:2 stoichiometry for **9d**-Cu^{2+} complex.

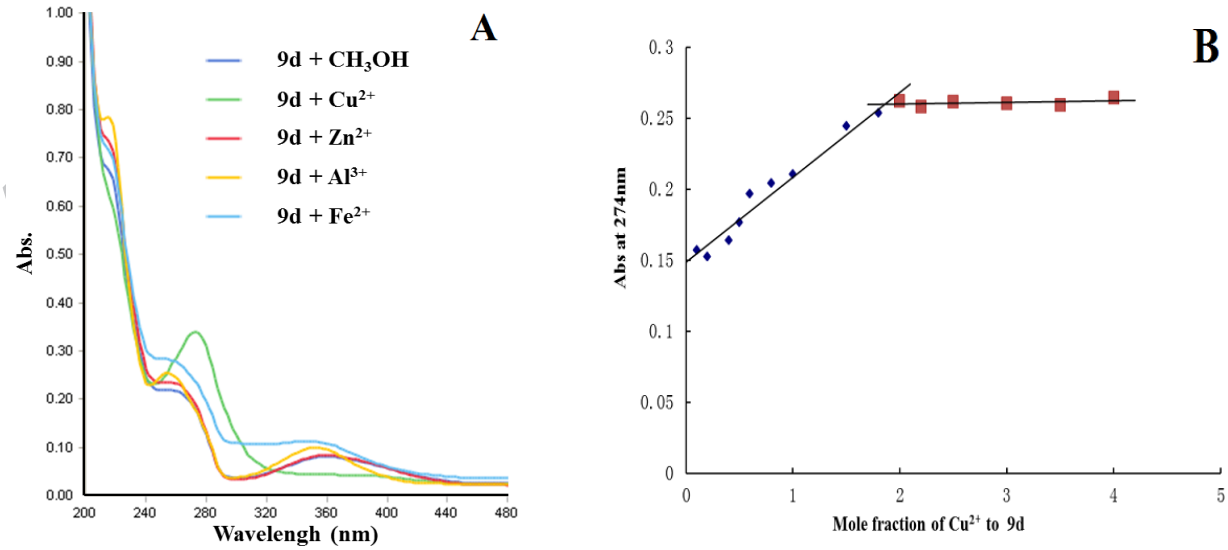

Figure 4. UV spectra of compound **9d** (**A**) (37.5 μM in methanol) alone or in the presence of $CuCl_2$,

$ZnCl_2$, $FeSO_4$ or $AlCl_3$ (37.5 μM, in methanol). Determination of the stoichiometry of complex-Cu^{2+} by using the molar ratio method of titrating the methanol solution of compound **9d** (**B**) with ascending amounts of $CuCl_2$. The final concentration of tested compound was 37.5 μM, and the final concentration of Cu^{2+} ranged from 3.75 to 150 μM.

2.2.6 Inhibition of self- and Cu^{2+}-induced Aβ_{1-42} aggregation of DHTA derivatives

The inhibitory activities of the target compounds on self- and Cu^{2+}-induced Aβ_{1-42} aggregation were determined by a thioflavin T (ThT) fluorescence assay, with curcumin as a reference compound.[37-40] The results summarized in **Table 2** indicated that all of the DHTA derivatives showed excellent inhibitory effects on self- and Cu^{2+}-induced Aβ_{1-42} aggregation (71.6~99.9% and 57.6~89.9% at 25 μM respectively), compared with curcumin (40.2 ± 0.9% and 66.0 ± 1.3% respectively). In view of the excellent self-induced Aβ_{1-42} aggregation inhibition activity of DHTA derivatives, we further determined their IC_{50} values, and the results were all at micromolar level (2.31-5.47 μM). However, compounds **3** and **4** almost had no inhibitory activity on Aβ_{1-42} aggregation inhibition at 25μM, indicating that the introduction of benzyl-alkyl side chain could indeed enhance their Aβ_{1-42} aggregation inhibitory activities. By comparison with lead compound Memoquin (IC_{50} = 5.93 ± 0.33 μM),[25] all of the derivatives exhibited better inhibitory activities. Different from the conclusion of AChE inhibition assay, the different alkyl side chain length and species of terminal benzylamines had no significant influence on the aggregation inhibition activity, and no obvious regularity of structure-activity relationship had been found.

Table 2. *In vitro* inhibition of Aβ_{1-42} aggregation and disaggregation of Aβ_{1-42} aggregation fibrils by DHTA derivatives and reference compound.

Compd.	n	% Inhibition of Aβ_{1-42} aggregation[a]		IC_{50} (μM) self-induced aggregation[d]
		Self-induced[b,d]	Cu^{2+}-induced[c,d]	
3	—	6.5 ± 0.2	30.7 ± 1.2	n.t.[e]
4	—	4.7 ± 0.1	8.1 ± 0.2	n.t.[e]
8a	3	85.0 ± 1.8	81.2 ± 3.3	3.98 ± 0.10
8b	3	81.0 ± 2.0	57.6 ± 2.0	4.20 ± 0.16
8c	3	93.5 ± 2.6	70.4 ± 2.8	3.63 ± 0.08
8d	3	98.2 ± 3.0	88.8 ± 4.2	2.41 ± 0.06
9a	4	90.0 ± 1.1	77.6 ± 2.6	3.55 ± 0.09

9b	4	88.0 ± 2.9	84.1 ± 1.7	3.86 ± 0.13
9c	4	98.6 ± 2.2	65.4 ± 2.9	3.45 ± 0.06
9d	4	96.2 ± 1.9	71.7 ± 3.0	3.05 ± 0.12
9e	4	99.7 ± 4.0	69.4 ± 3.3	3.71 ± 0.11
9f	4	99.9 ± 3.3	82.5 ± 4.0	3.16 ± 0.07
9g	4	71.6 ± 1.7	74.0 ± 1.0	5.47 ± 0.10
10a	6	99.8 ± 2.9	89.1 ± 2.6	2.37 ± 0.04
10b	6	91.4 ± 2.0	74.3 ± 1.8	2.80 ± 0.03
10c	6	99.7 ± 4.1	85.3 ± 2.1	2.31 ± 0.05
10d	6	99.6 ± 2.6	89.9 ± 2.4	3.31 ± 0.09
Curcumin	—	40.2 ± 0.9	66.0 ± 1.3	n.t.[e]

[a] For inhibition of Aβ aggregation assay, the thioflavin-T fluorescence method was used.

[b] Inhibition of self-induced A$\beta_{1\text{-}42}$ aggregation (25 μM) by tested inhibitors at 25 μM.

[c] Inhibition of Cu^{2+}-induced A$\beta_{1\text{-}42}$ aggregation. The concentration of tested compounds and Cu^{2+} were 25 μM.

[d] Data are presented as the mean ± SD of three independent experiments.

[e] n.t. = not tested.

2.2.7 Effect on the disaggregation of Aβ$_{1\text{-}42}$ aggregation fibrils of DHTA derivatives

Subsequently, we still used ThT method to determine the disaggregation ability to the formed Aβ fibers with DHTA derivatives. The results were summarized in **Table 3**. The results showed that DHTA derivatives also manifested good disaggregation ability to self- induced A$\beta_{1\text{-}42}$ aggregation fibrils. Similarly, the length of alkyl side chain and the type of terminal benzylamine moieties had little effect on the activity. It showed that the designed DHTA derivatives could not only inhibit A$\beta_{1\text{-}42}$ aggregation, but also depolymerize the polymeric protein fiber, with the potency to suppress and eliminate Aβ deposit plaque in AD brain, or to prevent and treat AD.

Table 3. *In vitro* disaggregation of A$\beta_{1\text{-}42}$ aggregation fibrils by DHTA derivatives and reference compound.

Compd.	n	% Disaggregation of A$\beta_{1\text{-}42}$ aggregation[a]	
		Self-induced[b,d]	Cu^{2+}-induced[c,d]
8a	3	68.5 ± 1.2	71.3 ± 1.7
8b	3	62.7 ± 1.6	70.6 ± 1.9
8c	3	70.1 ± 2.2	73.5 ± 2.5
8d	3	77.3 ± 2.6	73.1 ± 3.0

9a	4	67.7 ± 2.3	77.9 ± 3.1
9b	4	81.1 ± 3.0	80.0 ± 2.9
9c	4	80.3 ± 3.3	76.3 ± 2.6
9d	4	75.2 ± 3.1	77.2 ± 1.6
9e	4	64.4 ± 1.1	83.3 ± 2.1
9f	4	60.4 ± 2.0	84.7 ± 1.9
9g	4	67.4 ± 1.5	85.3 ± 2.3
10a	6	80.9 ± 2.7	89.3 ± 2.4
10b	6	83.5 ± 2.3	82.3 ± 3.1
10c	6	76.3 ± 1.4	89.8 ± 4.0
10d	6	83.8 ± 1.6	85.3 ± 3.2
Curcumin	—	n.t.[e]	54.7 ± 1.0

[a] For disaggregation of Aβ aggregation fibrils, the thioflavin-T fluorescence method was used.

[b] For disaggregation of self-induced A$\beta_{1\text{-}42}$ aggregation fibrils, the concentration of tested compounds and A$\beta_{1\text{-}42}$ were 25 μM.

[c] For disaggregation of Cu^{2+}-induced A$\beta_{1\text{-}42}$ aggregation fibrils, the concentration of tested compounds and Cu^{2+} were 25 μM.

[d] Data are presented as the mean ± SD of three independent experiments.

[e] n.t. = not tested.

2.2.8 Evaluation of in vitro blood-brain barrier (BBB) permeability

Passing the blood-brain barrier (BBB) and reaching the therapeutic targets is critical for drugs to act on neurodegenerative processes. The parallel artificial membrane permeation assay of the blood-brain barrier (PAMPA-BBB) was performed in order to determine the BBB permeability of the target compound.[41] First, the experimental permeabilities of 11 commercial drugs with reported values were compared to verify the assay (**Table S1**, Supplementary Material). The results of experimental data consistent with bibliographic values gave a strong linear correlation: P_e (exp.) = 0.9163 × P_e (bibl.) − 0.2247 (R^2 = 0.9558) (**Figure S1**, Supplementary Material). From this formula as well as the limit established by Di *et al.*[42] for BBB permeation, we determined that compounds with P_e values above 3.44 × 10^{-6} cm/s could cross the BBB (**Table S2**, Supplementary Material). As it shown in **Table 4**, compound **8d**, **9d** and **10d** had moderate BBB permeabilities and would be able to reach the therapeutic targets in central nervous system (CNS).

Table 4. Permeability results P_e (× 10^{-6} cm/s) from the PAMPA-BBB assay for selected DHTA derivatives with their predicted penetration into the CNS.

Compd.[a]	P_e (× 10^{-6} cm/s)[b]	Prediction
8d	4.23 ± 0.09	CNS +
9d	4.45 ± 0.11	CNS +
10d	5.54 ± 0.16	CNS +

[a] Compounds **8d, 9d** and **10d** were dissolved in DMSO at 5 mg/mL and diluted with PBS/EtOH (70:30). The final concentration of each compound was 100 μg/mL.

[b] Data are the mean ± SD of three independent experiments.

2.2.9 Evaluation of in vitro anti-neuroinflammatory activities of DHTA derivatives

Neuroinflammation in AD is mainly characterized by the activation of microglia in the brain and the release of multiple proinflammatory cytokines. To evaluate the anti-neuroinflammatory activity of the target compounds, representative compounds **8d**, **9c**, **9d**, **10d** and parent compound **4** were tested with the inflammatory microglial BV-2 cells stimulated by lipopolysaccharide (LPS). Flurbiprofen was used as reference compound. The *in vitro* neurocytotoxicity, inhibition of LPS induced NO and TNF-*α* production were investigated.[43-46]

2.2.9.1 Effects of compounds on the survival rate of BV-2 microglial

First, we used MTT method to determine the cytotoxicity of representative compounds without or with LPS on the BV-2 microglia cells. As the results shown in **Figure 5**, whether added LPS (1.0 μg/mL) or not, cell viability did almost not change after treatment with various concentrations (0.5, 2.5 and 10.0 μM) of the compounds. It indicated compound **4**, **8d**, **9c**, **9d**, **10d** and flurbiprofen have no cytotoxicity toward the BV-2 cell at concentrations below 10 μM, and LPS (1.0 μg/mL) could not alter cell viability also.

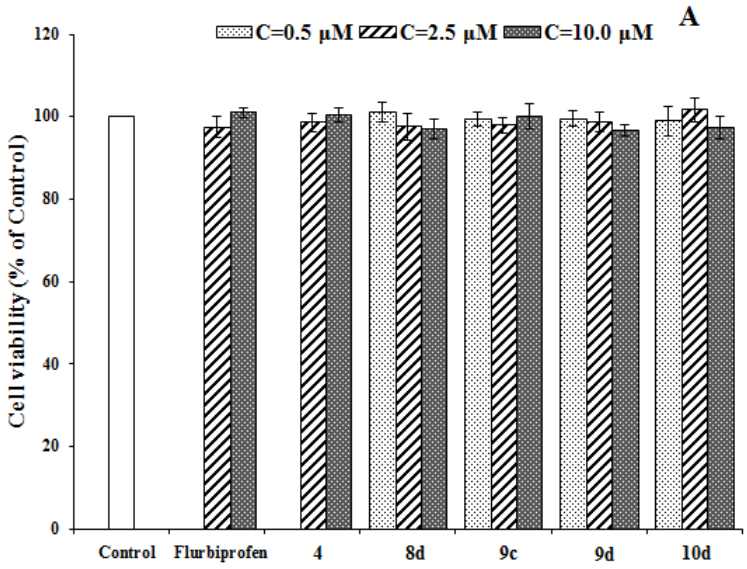

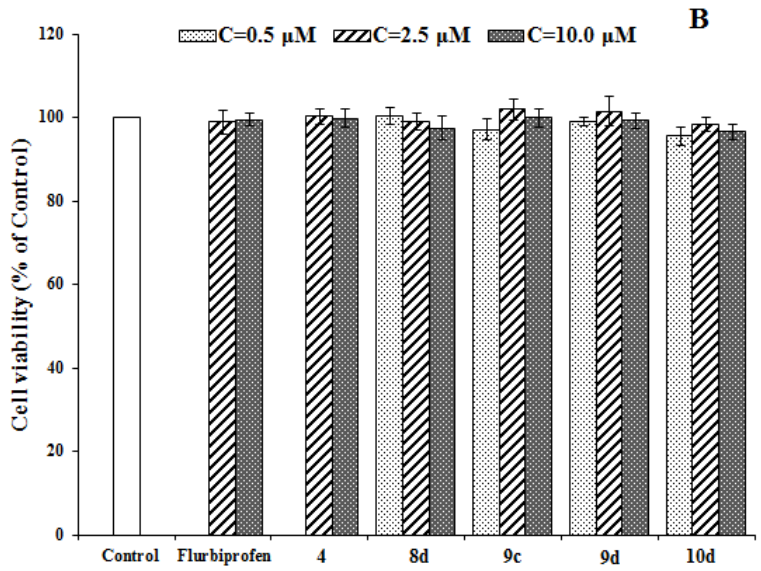

Figure 5. Effects of compound **4**, **8d**, **9c**, **9d**, **10d** and flurbiprofen without LPS (**A**) or with LPS (**B**) on the cell viability of microglia BV-2 cells. BV-2 cells were pre-incubated with indicated concentrations of compounds for 30 min followed by 1.0 μg/mL LPS treatment for 24 h. Cell viability was determined by MTT assay. The data are expressed as the mean ± SD from three independent experiments.

2.2.9.2 Effects of compounds on the release of NO in LPS-stimulated BV-2 cells

Inhibition of LPS-induced NO production was measured by using Griess reaction method. First, we examined the effect of compound itself on NO release from BV-2 cells without LPS. As shown in **Figure 6**, NO release volume didn't change a lot compared with the control group, so compounds **8d**, **9c**, **9d** and **10d** had no effect on it. Then in LPS-treated cells, we observed a massive induction of NO production, which was significantly reduced by treatment with compounds in a dose-dependent manner. Compared with reference compound flurbiprofen (11.8% and 23.0% when the cells were treated with 2.5 and 10.0 μM), representative compounds showed good inhibitory activity on LPS-induced NO production. **8d**, **9c**, **9d** and **10d** displayed better NO inhibitory activity with the respective percentages of 35.0%, 36.7%, 30.0% and 33.3% when the cells were treated with 2.5 μM. They also showed excellent inhibitory activity with the respective percentages of 50.8%, 57.5%, 58.3% and 63.3% when the cells were treated with 10.0 μM. Moreover, the entire representative compounds showed far better activities in comparison with the parent compound **4** (8.3% and 12.5% when the cells were treated with 2.5 and 10.0 μM). It indicated that the introduction of

alkylbenzylamine group by the amidation of carboxyl groups was beneficial to the reduction of NO release in LPS-stimulated BV-2 cells.

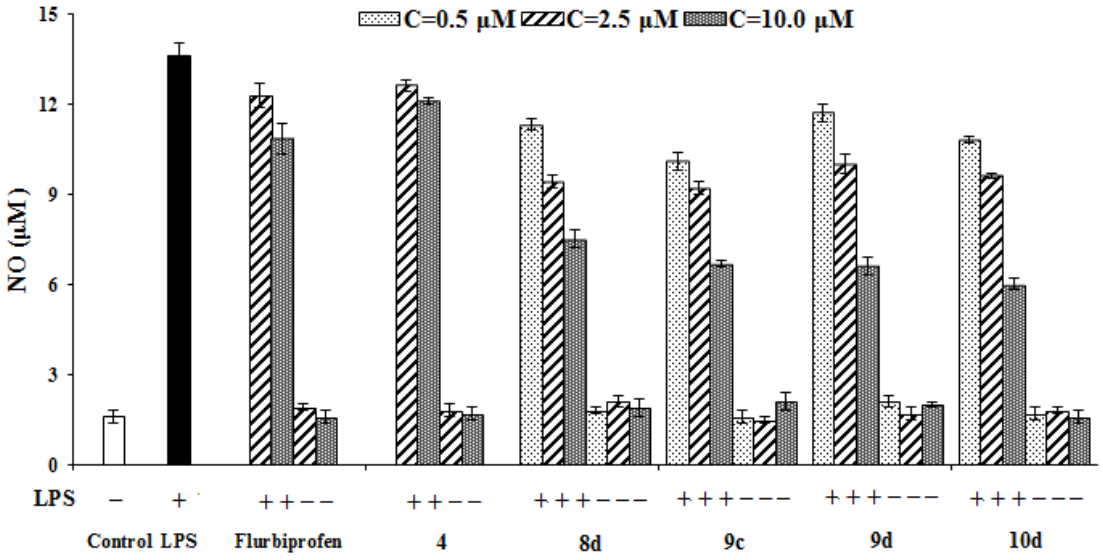

Figure 6. Effects of compounds **4**, **8d**, **9c**, **9d**, **10d** and flurbiprofen on NO release in BV-2 cells and LPS-stimulated BV-2 cells. The data are expressed as the mean ± SD from three independent experiments.

2.2.9.3 Effects of compounds on TNF-α in LPS-stimulated BV-2 cells

Inhibition of LPS-induced TNF-α production was measured by the enzyme-linked immunosorbent assay (ELISA). The result was shown in **Figure 7**. First we could also find that compound **8d**, **9c**, **9d** and **10d** had no effect on TNF-α production without added LPS up to the concentration of 10 μM. Then in the LPS-treated cells, the amount of TNF-*α* released in the BV-2 cells increased significantly. It was also reduced by treatment with compounds at the concentration of 0.5-10 μM in a dose-dependent manner. Compared with the reference compound flurbiprofen (9.6% and 30.3% when the cells were treated with 2.5 and 10.0 μM), all the representative compounds showed much better inhibitory activities on LPS-induced TNF-*a* production. The inhibition activity of the compounds was relatively weak at 0.5 μM, and they showed moderate activities at 2.5 μM with the respective percentages of 28.2%, 32.9%, 37.1% and 20.6%. In addition, the cells were treated with 10.0 μM, **8d**, **9c**, **9d** and **10d** displayed good inhibitory activity with the respective percentages of 41.1%, 59.4%, 55.3% and 50.6%. Moreover, all the representative compounds showed better activities in comparison with the parent compound **4** (5.9% and 18.2% when the cells

were treated with 2.5 and 10.0 μM).

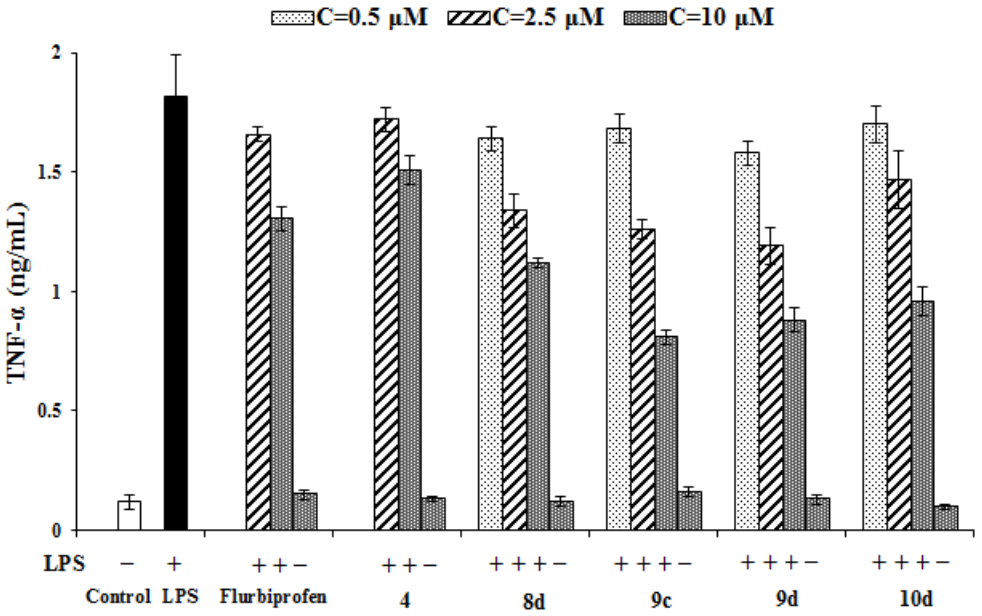

Figure 7. Effects of compounds **4**, **8d**, **9c**, **9d**, **10d** and flurbiprofen on TNF-α release in LPS-stimulated BV-2 cells. The data are expressed as the mean ± SD from three independent experiments.

Collectively, representative compounds **8d**, **9c**, **9d** and **10d** had no obvious toxicity to BV-2 cells at their effective concentration, and could not promote inflammatory effects to the activate microglial cells. It may indicate certain medicinal safety of these compounds. And they also had significant inhibitory activities on NO and TNF-α production in LPS-stimulated BV-2 cells, which was beneficial to relieve the neuroinflammation in the brain of neurodegenerative disease.

3. Conclusion

In summary, a series of DHTA derivatives were designed, synthesized and evaluated as multifunctional agents for the treatment of AD. *In vitro* assays demonstrated that most of the synthesized compounds were potent in inhibiting AChE activity and displayed high selectivity for AChE over BuChE. They showed significant inhibitory activities of self- and Cu^{2+}-induced Aβ_{1-42} aggregation, moderate antioxidant activities and good anti-inflammatory properties. Among them, compound **9d** exhibited a useful inhibitory activity toward AChE with IC_{50} value of 0.56 μM. The kinetic analysis suggested that **9d** showed mixed-type inhibition, and could bind to both CAS and PAS of AChE, which was consistent with the molecular modeling study. In addition, **9d** displayed

good self- and Cu^{2+}-induced Aβ_{1-42} aggregation inhibitory potency (96.2% and 71.7% at 25 μM, respectively), and the IC_{50} value of self-induced Aβ_{1-42} aggregation was 3.05 μM. Moreover, **9d** also showed good disaggregation ability to self- and Cu^{2+}-induced Aβ_{1-42} aggregation fibrils (75.2% and 77.2% at 25 μM, respectively), moderate antioxidant activity and good biometal chelating ability. Furthermore, **9d** possessed the prospective properties of acting as anti-neuroinflammatory agent. More importantly, **9d** could cross the BBB and penetrate into brain. The IC_{50} values of its various activities are basically at the micromole level, and the activities are relatively balanced. These multifunctional properties highlight compound **9d** as a promising candidate for further studies directed to the development of novel drugs against AD.

4. Experimental section

4.1 Chemistry

All materials, unless otherwise noted, were of analytical reagent grade and purchased from commercial suppliers. Thin-layer chromatography (TLC) was performed on silica gel GF_{254} plates from Qingdao Haiyang Chemical Co. Ltd. (China). The spots were detected by UV light (254 nm). Column chromatography was performed using silica gel (230-400 mesh) purchased from Qingdao Haiyang Chemical Co. Ltd. (China). Melting points were measured with YRT-3 melting-point apparatus (China) and uncorrected. HPLC analysis was carried out on a Shimadzu LC-10Avp plus system using a Kromasil C_{18} column (4.6 mm × 250 mm, 5 μm). The ^{1}H NMR and ^{13}C NMR spectra were recorded in $CDCl_3$ or DMSO-d_6 on a Varian INOVA spectrometer at 25 °C with TMS as the internal standard. Coupling constants are given in Hz. Mass spectra were recorded on Agilent-6210 TOF LC-MS Spectrometer.

*4.1.1. Diethyl 2,5-dioxocyclohexane-1,4-dicarboxylate (**2**)*

Sodium crumb (5.82 g, 253 mmol) was added in ethanol (60 mL) at room temperature, and then the reaction mixture was refluxed until the solid was dissolved. Diethyl succinate (**1**, 20 mL, 119 mmol) was added in the freshly prepared sodium ethanol/ethanol reagent. The mixture was refluxed for another 5 h. Ethanol was removed under reduced pressure. The residue was acidified with 2N sulfuric acid until the pH was about 2 with the precipitation of yellow solid. The reaction mixture was stirred at room temperature for 5 h. The precipitate was filtered, washed with water and dried at

room temperature to afford crude product **2** which was recrystallized with ethyl acetate to obtain off-white crystalline solid (9.25 g, 60.4%). mp 128-129 °C (Lit.[26] 128 °C)

*4.1.2. Diethyl 2,5-dihydroxyterephthalate (**3**)*

The suspension of compound **2** (9.25 g, 36.1 mmol) in glacial acetic acid (60 mL) was heated at 60 °C until the solid was dissolved. N-chlorosuccinimide (4.90 g, 36.7 mmol) was added in portions .After that the reaction was heated at 80 °C for 5 h, and then cooled to room temperature with a large amount of crystals precipitating. After filtration, the filter cake was washed with cold methanol and dried at room temperature to give compound **3** (8.16 g 89.0%) as yellow columnar crystals. mp 134-135 °C (Lit.[27] 133-134 °C). ^{1}H NMR (400 MHz, $CDCl_3$) δ 10.15 (s, 2H), 7.48 (s, 2H), 4.42 (q, J = 7.2 Hz, 4H), 1.43 (t, J = 7.2 Hz, 6H).

*4.1.3. 2,5-Dihydroxyterephthalic acid (**4**)*

The mixture of compound **3** (2.00 g, 7.87 mmol) and sodium hydroxide (1.61 g, 40.3 mmol) in water (40 mL) was heated at 80 °C under argon protection for 5 h. The reaction solution was cooled to room temperature, and the pH was adjusted to approximately 1.0 with concentrated hydrochloric acid. A large amount of bright yellow solids were precipitated, and the mixture was stirred at room temperature for 1 h. The mixture was filtered, and the filter cake was washed with water until neutral and dried at room temperature to obtain crude product **4** (1.50 g, 96.2%) as a bright yellow solid which was used without further purification. ^{1}H NMR (400 MHz, DMSO-d_6) δ 10.59 (brs, 2H), 7.29 (s, 2H), 3.96 (brs, 2H).

*4.1.4. General procedure for the synthesis of **8-10***

To a stirred solution of compound **4** (50 mg, 0.252 mmol), EDCI (169 mg, 0.882 mmol), HOBt (119 mg, 0.881 mmol) and triethylamine (0.176 mL, 1.26 mmol) in tetrahydrofuran (3 mL), corresponding primary amines **5–7** (0.882 mmol) was added. The reaction mixture was stirred at room temperature overnight. After the reaction was completed, the mixture was concentrated. Then dichloromethane (15 mL) was added to the residue and the mixture was washed with saturated aqueous sodium bicarbonate solution (10 mL) and brine (10 mL), dried over sodium sulfate, filtered and concentrated under reduced pressure to give the crude compound. The obtained residue was purified by silica gel column chromatography to afford **8–10**.

*4.1.4.1. N^1,N^4-bis(3-(benzyl(methyl)amino)propyl)-2,5-dihydroxyterephthalamide (**8a**)*

Compound **8a** was synthesized from intermediate **4** and **5a** according to the general procedure. After purification by chromatography on silica gel using dichloromethane/acetone (1:3) as eluent, the pure product **8a** was obtained as yellow oil, yield 62.6%. ^{1}H NMR (400 MHz, $CDCl_3$) δ 11.80 (brs,

2H), 8.76 (brs, 2H), 7.33-7.26 (m, 10H), 6.87 (s, 2H), 3.64 (s, 4H), 3.55-3.45 (m, 4H), 2.65-2.60 (m, 4H), 2.39 (s, 6H), 1.86-1.79 (m, 4H); ^{13}C NMR (100 MHz, $CDCl_3$) δ 168.7, 152.7, 136.9, 129.4, 128.6, 127.6, 119.2, 114.3, 62.9, 56.1, 41.8, 40.0, 24.6. ESI-MS m/z: 519.4 $[M+H]^+$.

*4.1.4.2. N^1,N^4-bis(3-(benzyl(ethyl)amino)propyl)-2,5-dihydroxyterephthalamide (**8b**)*

Compound **8b** was synthesized from intermediate **4** and **5b** according to the general procedure. After purification by chromatography on silica gel using dichloromethane/acetone (1:3) as eluent, the pure product **8b** was obtained as yellow oil, yield 44.5%. ^{1}H NMR (400 MHz, $CDCl_3$) δ 11.73 (brs, 2H), 8.55 (brs, 2H), 7.37-7.26 (m, 10H), 6.91 (s, 2H), 3.70 (s, 4H), 3.50-3.45 (m, 4H), 2.75-2.65 (m, 8H), 1.85-1.76 (m, 4H), 1.19 (t, J = 7.2Hz, 6H); ^{13}C NMR (100 MHz, $CDCl_3$) δ 168.8, 152.6, 137.1, 129.4, 128.5, 127.6, 119.1, 114.5, 58.0, 51.9, 47.1, 39.7, 24.5, 10.9. ESI-MS m/z: 547.3 $[M+H]^+$.

*4.1.4.3. 2,5-Dihydroxy-N^1,N^4-bis(3-((2-methoxybenzyl)(methyl)amino)propyl)terephthalamide (**8c**)*

Compound **8c** was synthesized from intermediate **4** and **5c** according to the general procedure. After purification by chromatography on silica gel using dichloromethane/acetone (1:5) as eluent, the pure product **8c** was obtained as yellow oil, yield 48.4%. ^{1}H NMR (400 MHz, $CDCl_3$) δ 11.50 (brs, 2H), 9.23 (brs, 2H), 7.31-7.27 (m, 4H), 6.94-6.91 (m, 4H), 6.84 (d, J = 8.0 Hz, 2H), 3.76 (s, 4H), 3.68 (s, 6H), 3.51-3.47 (m, 4H), 2.85-2.75 (m, 4H), 2.43 (s, 6H), 1.95-1.84 (m, 4H); ^{13}C NMR (100 MHz, $CDCl_3$) δ 168.7, 157.9, 152.6, 131.8, 129.4, 124.4, 120.2, 119.1, 114.4, 110.7, 57.1, 56.6, 55.0, 41.7, 40.2, 24.5. ESI-MS m/z: 579.3 $[M+H]^+$.

*4.1.4.4. N^1,N^4-bis(3-(ethyl(2-methoxybenzyl)amino)propyl)-2,5-dihydroxyterephthalamide (**8d**)*

Compound **8d** was synthesized from intermediate **4** and **5d** according to the general procedure. After purification by chromatography on silica gel using dichloromethane/acetone (1:5) as eluent, the pure product **8d** was obtained as yellow oil, yield 47.3%. ^{1}H NMR (400 MHz, $CDCl_3$) δ 11.80 (brs, 2H), 9.07 (brs, 2H), 7.30-7.26 (m, 4H), 6.94-6.90 (m, 4H), 6.84 (d, J = 8.4 Hz, 2H), 3.75 (s, 4H), 3.70 (s, 6H), 3.47-3.44 (m, 4H), 2.80-2.70 (m, 8H), 1.90-1.78 (m, 4H), 1.16 (t, J = 6.4 Hz, 6H); ^{13}C NMR (100 MHz, $CDCl_3$) δ 168.7, 157.9, 152.4, 131.7, 129.3, 124.6, 120.3, 119.0, 114.6, 110.7, 55.0, 52.5, 52.4, 47.4, 40.1, 24.3, 10.2. ESI-MS m/z: 607.4 $[M+H]^+$.

*4.1.4.5. N^1,N^4-bis(4-(benzyl(methyl)amino)butyl)-2,5-dihydroxyterephthalamide (**9a**)*

Compound **9a** was synthesized from intermediate **4** and **6a** according to the general procedure. After purification by chromatography on silica gel using dichloromethane/acetone (1:4) as eluent, the pure product **9a** was obtained as yellow oil, yield 45.2%. ^{1}H NMR (400 MHz, $CDCl_3$) δ 11.01 (brs,

2H), 8.00 (brs, 2H), 7.32-7.26 (m, 10H), 7.01 (s, 2H), 3.61 (s, 4H), 3.43-3.37 (m, 4H), 2.48-2.42 (m, 4H), 2.27 (s, 6H), 1.70-1.65 (m, 8H). ESI-MS m/z: 547.3 $[M+H]^+$.

*4.1.4.6. N^1,N^4-bis(4-(benzyl(ethyl)amino)butyl)-2,5-dihydroxyterephthalamide (**9b**)*

Compound **9b** was synthesized from intermediate **4** and **6b** according to the general procedure. After purification by chromatography on silica gel using dichloromethane/methanol (8:1) as eluent, the pure product **9b** was obtained as yellow oil, yield 65.7%. ^{1}H NMR (400 MHz, $CDCl_3$) δ 8.67 (brs, 2H), 7.76 (brs, 2H), 7.39-7.25 (m, 10H), 7.18 (s, 2H), 3.78 (s, 4H), 3.40 (t, J = 6.0 Hz, 4H), 2.71 (q, J = 7.2 Hz, 4H), 2.65 (t, J = 6.8 Hz, 4H), 1.71-1.63 (m, 8H), 1.14 (t, J = 7.2 Hz, 6H); ^{13}C NMR (100 MHz, $CDCl_3$) δ 168.6, 152.1, 135.8, 129.6, 128.5, 127.8, 119.5, 115.0, 57.3, 52.1, 47.0, 39.2, 26.8, 23.6, 10.5. ESI-MS m/z: 575.4 $[M+H]^+$.

*4.1.4.7. 2,5-Dihydroxy-N^1,N^4-bis(4-((2-methoxybenzyl)(methyl)amino)butyl)terephthalamide (**9c**)*

Compound **9c** was synthesized from intermediate **4** and **6c** according to the general procedure. After purification by chromatography on silica gel using dichloromethane/acetone (1:5) as eluent, the pure product **9c** was obtained as yellow oil, yield 39.1%. ^{1}H NMR (400 MHz, $CDCl_3$) δ 8.59 (brs, 2H), 7.27-7.24 (m, 4H), 7.03 (s, 2H), 6.92 (t, J = 7.2 Hz, 2H), 6.85 (d, J = 8.4 Hz, 2H), 3.76 (s, 6H), 3.67 (s, 4H), 3.38-3.34 (m, 4H), 2.52-2.48 (m, 4H), 2.30 (s, 6H), 1.73-1.67 (m, 8H); ^{13}C NMR (100 MHz, $CDCl_3$) δ 168.8, 157.9, 152.3, 131.7, 129.1, 124.5, 120.2, 119.4, 114.6, 110.4, 56.6, 55.7, 55.1, 42.7, 39.3, 26.7, 24.4. ESI-MS m/z: 607.3 $[M+H]^+$.

*4.1.4.8. N^1,N^4-bis(4-(ethyl(2-methoxybenzyl)amino)butyl)-2,5-dihydroxyterephthalamide (**9d**)*

Compound **9d** was synthesized from intermediate **4** and **6d** according to the general procedure. After purification by chromatography on silica gel using dichloromethane/acetone (1:4) as eluent, the pure product **9d** was obtained as yellow oil, yield 47.5%. ^{1}H NMR (400 MHz, $CDCl_3$) δ 7.99 (brs, 2H), 7.37 (d, J = 7.2 Hz, 2H), 7.26-7.23 (m, 2H), 7.06 (s, 2H), 6.92 (t, J = 7.2 Hz, 2H), 6.84 (d, J = 8.4 Hz, 2H), 3.79 (s, 6H), 3.76 (s, 4H), 3.37 (t, J = 6.0 Hz, 4H), 2.71 (q, J = 6.8 Hz, 4H), 2.62 (t, J = 6.0 Hz, 4H), 1.71-1.65 (m, 8H), 1.12 (t, J = 6.8 Hz, 6H, 2 × CH_3); ^{13}C NMR (100 MHz, $CDCl_3$) δ 168.5, 157.8, 152.1, 131.3, 129.0, 124.3, 120.4, 119.6, 115.1, 110.4, 55.0, 52.3, 51.3, 47.6, 39.2, 26.9, 23.9, 10.4. ESI-MS m/z: 635.4 $[M+H]^+$.

*4.1.4.9. N^1,N^4-bis(4-((2-(dimethylamino)benzyl)(ethyl)amino)butyl)-2,5-dihydroxyterephthalamide (**9e**)*

Compound **9e** was synthesized from intermediate **4** and **6e** according to the general procedure.

After purification by chromatography on silica gel using dichloromethane/acetone (1:6) as eluent, the pure product **9e** was obtained as yellow oil, yield 31.9%. ^{1}H NMR (400 MHz, $CDCl_3$) δ 8.56 (brs, 2H), 8.00 (brs, 2H), 7.58 (d, J = 7.2 Hz, 2H), 7.29 (s, 2H), 7.24 (t, J = 8.0 Hz, 2H), 7.16 (d, J = 8.0 Hz, 2H), 7.05 (t, J = 7.2 Hz, 2H), 3.88 (s, 4H), 3.40-3.37 (m, 4H), 2.73-2.64 (m, 8H), 2.64 (s, 12H), 1.67-1.62 (m, 8H), 1.11 (t, J = 6.8 Hz, 6H); ^{13}C NMR (100 MHz, $CDCl_3$) δ 168.4, 153.1, 151.9, 130.7, 130.3, 128.5, 123.7, 119.9, 119.5, 115.5, 52.5, 52.3, 47.4, 45.2, 39.1, 26.7, 23.5, 10.4. ESI-MS m/z 661.4 $[M+H]^+$.

*4.1.4.10. N^1,N^4-bis(4-((4-(dimethylamino)benzyl)(ethyl)amino)butyl)-2,5-dihydroxyterephthalamide (**9f**)*

Compound **9f** was synthesized from intermediate **4** and **6f** according to the general procedure. After purification by chromatography on silica gel using dichloromethane/acetone (1:6) as eluent, the pure product **9f** was obtained as yellow oil, yield 37.7%. ^{1}H NMR (400 MHz, $CDCl_3$) δ 8.61 (brs, 4H), 7.30 (s, 2H), 7.22 (d, J = 8.4 Hz, 4H), 6.63 (d, J = 8.4 Hz, 4H), 3.80 (s, 4H), 3.40 (t, J = 5.6 Hz, 4H), 2.90 (s, 12H), 2.77 (q, J = 6.8 Hz, 4H), 2.70 (t, J = 6.8 Hz, 4H), 1.82-1.72 (m, 4H), 1.68-1.58 (m, 4H), 1.19 (t, J = 6.8 Hz, 6H); ^{13}C NMR (100 MHz, $CDCl_3$) δ 168.6, 152.0, 150.4, 131.1, 120.0, 119.7, 115.6, 112.2, 56.4, 51.5, 46.6, 40.3, 38.9, 26.6, 22.9, 9.9. ESI-MS m/z: 661.4 $[M+H]^+$.

4.1.4.11.

*N^1,N^4-bis(4-(2,3-dihydrobenzo[f][1,4]oxazepin-4(5H)-yl)butyl)-2,5-dihydroxyterephthalamide (**9g**)*

Compound **9g** was synthesized from intermediate **4** and **6g** according to the general procedure. After purification by chromatography on silica gel using dichloromethane/acetone (1:3) as eluent, the pure product **9g** was obtained as yellow oil, yield 55.3%. ^{1}H NMR (400 MHz, $CDCl_3$) δ 11.20 (brs, 2H), 7.63 (brs, 2H), 7.19 (t, J = 8.0 Hz, 2H), 7.13 (d, J = 7.2 Hz, 2H), 7.01 (s, 2H), 7.01-6.98 (m, 4H), 4.09 (ts, J = 4.0 Hz, 4H), 3.92 (s, 4H), 3.47-3.41 (m, 4H), 3.17 (ts, J = 4.0 Hz, 4H), 2.55 (t, J = 6.4 Hz, 4H), 1.73-1.64 (m, 8H); ^{13}C NMR (100 MHz, DMSO-d_6) δ 165.9, 157.7, 149.6, 129.7, 128.9, 126.6, 121.3, 118.5, 117.9, 113.7, 67.7, 55.9, 55.7, 51.1, 37.2, 24.7, 22.4. ESI-MS m/z: 603.3 $[M+H]^+$.

*4.1.4.12. N^1,N^4-bis(6-(benzyl(methyl)amino)hexyl)-2,5-dihydroxyterephthalamide (**10a**)*

Compound **10a** was synthesized from intermediate **4** and **7a** according to the general procedure. After purification by chromatography on silica gel using dichloromethane/acetone (1:3) as eluent, the pure product **10a** was obtained as yellow oil, yield 47.2%. ^{1}H NMR (400 MHz, $CDCl_3$) δ 7.33-7.26

(m, 10H), 7.09 (s, 2H), 6.76 (brs, 2H), 3.57 (s, 4H), 3.42 (q, *J* = 6.8 Hz, 4H), 2.43 (t, *J* = 7.6 Hz, 4H), 2.25 (s, 6H), 1.61-1.57 (m, 8H), 1.38-1.32 (m, 8H). ESI-MS m/z: 603.4 $[M+H]^+$.

*4.1.4.13. N^1,N^4-bis(6-(benzyl(ethyl)amino)hexyl)-2,5-dihydroxyterephthalamide (**10b**)*

Compound **10b** was synthesized from intermediate **4** and **7b** according to the general procedure. After purification by chromatography on silica gel using dichloromethane/acetone (1:1) as eluent, the pure product **10b** was obtained as yellow oil, yield 44.0%. ^{1}H NMR (400 MHz, $CDCl_3$) δ 8.50 (brs, 2H), 7.61 (brs, 2H), 7.43-7.27 (m, 12H), 3.80 (s, 4H), 3.42-3.36 (m, 4H), 2.72 (q, *J* = 6.8 Hz, 4H), 2.61 (t, *J* = 7.6 Hz, 4H), 1.64-1.54 (m, 8H), 1.35-1.25 (m, 8H), 1.17 (t, *J* = 6.8 Hz, 6H); ^{13}C NMR (100 MHz, $CDCl_3$) δ 168.2, 151.8, 134.8, 129.7, 128.5, 128.0, 119.9, 115.6, 57.0, 52.2, 46.8, 39.5, 28.9, 26.5, 26.4, 25.1, 10.2. ESI-MS m/z: 631.4 $[M+H]^+$.

*4.1.4.14. 2,5-Dihydroxy-N^1,N^4-bis(6-((2-methoxybenzyl)(methyl)amino)hexyl)terephthalamide (**10c**)*

Compound **10c** was synthesized from intermediate **4** and **7c** according to the general procedure. After purification by chromatography on silica gel using dichloromethane/acetone (1:4) as eluent, the pure product **10c** was obtained as yellow oil, yield 49.2%. ^{1}H NMR (400 MHz, $CDCl_3$) δ 7.58 (brs, 2H), 7.39 (d, *J* = 7.2 Hz, 2H), 7.32-7.28 (m, 4H), 6.93 (t, *J* = 7.2 Hz, 2H), 6.87 (d, *J* = 8.4 Hz, 2H), 3.82 (s, 6H), 3.79 (s, 4H), 3.42-3.37 (m, 4H), 2.61 (t, *J* = 8.0 Hz, 4H), 2.39 (s, 6H), 1.68-1.54 (m, 8H), 1.36-1.30 (m, 8H); ^{13}C NMR (100 MHz, $CDCl_3$) δ 168.0, 157.9, 151.7, 131.8, 129.7, 122.2, 120.5, 120.3, 116.1, 110.5, 56.6, 55.3, 54.5, 41.0, 39.4, 28.9, 26.5, 26.4, 25.6. ESI-MS m/z: 663.4 $[M+H]^+$

*4.1.4.15. N^1,N^4-bis(6-(ethyl(2-methoxybenzyl)amino)hexyl)-2,5-dihydroxyterephthalamide (**10d**)*

Compound **10d** was synthesized from intermediate **4** and **7d** according to the general procedure. After purification by chromatography on silica gel using petroleum ether/acetone (1:2) as eluent, the pure product **10d** was obtained as yellow oil, yield 46.1%. ^{1}H NMR (400 MHz, $CDCl_3$) δ 7.44 (d, *J* = 7.2 Hz, 2H), 7.26-7.23 (m, 2H), 7.16 (s, 2H), 7.07 (brs, 2H), 6.94 (t, *J* = 7.2 Hz, 2H), 6.86 (d, *J* = 8.4 Hz, 2H), 3.82 (s, 6H), 3.74 (s, 4H), 3.42-3.39 (m, 4H), 2.66 (q, *J* = 6.8 Hz, 4H), 2.57 (t, *J* = 7.6 Hz, 4H), 1.62-1.54 (m, 8H), 1.38-1.30 (m, 8H), 1.12 (t, *J* = 6.8 Hz, 6H); ^{13}C NMR (100 MHz, $CDCl_3$) δ 168.1, 157.8, 151.9, 131.2, 129.1, 123.9, 120.5, 120.2, 115.7, 110.4, 55.3, 52.7, 50.9, 47.3, 39.5, 29.0, 26.7, 26.5, 25.5, 10.5. ESI-MS m/z: 691.5 $[M+H]^+$.

4.2. Biological evaluation

4.2.1. Evaluation of in vitro AChE and BuChE inhibitiory activity

In order to evaluate the *in vitro* cholinesterase (ChE) activities of the compounds, the Ellman's spectrophotometrical method was performed.[24,30] We used AChE from 5% rat cortex homogenate, purified AChE from *Electrophorus electricus* (Sigma-Aldrich Co.) and BuChE from rat serum. Before using the brain homogenate, it was preincubated with tetraisopropyl pyrophosphoramide (*iso*-OMPA, selective inhibitor of BuChE, 4.0 mmol/L, Sigma-Aldrich Co.) for 5 min. For the inhibition assays of rat AChE or BuChE, the reaction was initiated by adding 30 μL acetylthiocholine iodide (1 mmol/L) (J&K Scientific) or butyrylthiocholine iodide (1 mmol/L) (TCI Shanghai Development), 10 μL 5% homogenate or 25% serum, 20 μL different concentrations of test compounds and 40 μL phosphate-buffered solution (0.1 mmol/L, pH = 7.40). The mixture was then incubated at 37 °C for 15 min, and ended with the addition of 30 μL 5,5'-dithiobis-2-nitrobenzoic acid (DTNB, 0.2%) (J&K Scientific) to produce the yellow anion of 5-thio-2-nitrobenzoic acid. The absorbance was measured at 405 nm in a Varioskan Flash Multimode Reader (Thermo Scientific). For *Ee*AChE inhibition assay, *Ee*AChE was used at 0.05 U/mL (final concentration), and the assay was performed in a phosphate buffer (0.01 mmol/L, pH= 8.00). The absorbance was measured at 412 nm. The other procedure was the same as above. IC_{50} values were calculated as the concentration of compound that produces 50% inhibition of AChE or BuChE activity. Donepezil was applied as the positive drug. All samples were assayed in triplicate.

4.2.2. Evaluation of AChE inhibitor kinetics

Kinetic characterization of AChE inhibition was carried out based on a reported method using *Ee*AChE.[31] The assay solution consisted of 30 μL of 0.2% DTNB, 10 μL of 0.5 U/mL *Ee*AChE, 20 μL three different concentrations of inhibitors and 20 μL phosphate buffer (0.1 M, pH 8.00). The mixture was pre-incubated with the *Ee*AChE for 15 min at 37°C, followed by the addition of 20 μL TACh in different concentrations. The absorbance was measured at 412 nm. The parallel control experiments were performed without inhibitor. Slopes of reciprocal plots were then plotted against the concentration of **9d** in a weighted analysis, and K_i was determined as the intercept on the negative *x*-axis.

4.2.3. Molecular modeling study

The crystal structures of *Torpedo* AChE complexed with donepezil (PDB code: *1EVE*) and mouse AChE (mAChE, PDB code: 4B85) were obtained from the Protein Data Bank after removing

the original inhibitors and water molecules.[32] The 3D structure of **9d** was prepared as similarly as previously described.[28] Docking studies were performed using the AUTODOCK 4.2 program. The enzyme structure was used as an input for the AutoGrid program, after the addition of polar hydrogen atoms to amino acid residues and the distribution of Gasteiger charges to all atoms of the enzyme by using Autodock Tools (version 1.5.6). Precalculated grid maps were obtained using AutoGrid, one for each atom type present in the ligand. The grid point spacing for all maps is 0.375Å. The center of the grid box was located in the center of donepezil with coordinates x = 2.023, y = 63.295, z = 67.062. The size of box for the active site were set at 60 × 60 × 60 Å. Flexible ligand docking was performed for the compounds. Each docked system was executed through 100 runs of AutoDock searches conducted by the Lamarckian genetic algorithm (LGA). In addition to the above parameters, other parameters were accepted as default. The docking results were clustered using a root mean square (RMS) tolerance of 1.0, and the lowest energy conformation of the highest filled cluster was selected for analysis. Autodock Tools or Discovery Studio 2.5 software was used to complete graphic manipulations and visualizations.

4.2.4. Evaluation of antioxidant activity

The antioxidant *activity* was measured by the oxygen radical absorbance capacity-fluorescein (ORAC-FL) assay.[34] Fluorescein (FL) and 6-hydroxy-2,5,7,8-tetramethylchromane-2- carboxylic acid (Trolox) were purchased from TCI (Shanghai) Development. 2,2'-Azo-bis(amidinopropane) dihydrochloride (AAPH) was purchased from Accela ChemBio Co., Ltd. All the assays were performed with 75 mM phosphate buffer (pH = 7.40). 120 μL FL (150 nM final concentration) and 20 μL antioxidant were added in the wells of a black 96-well plate using Trolox as a standard (1-8 μM, final concentration). The plate was incubated for 15 min at 37 °C and then placed in a Varioskan Flash Multimode Reader (Thermo Scientific). 60 μL AAPH solution (12 mM final concentration) was quickly added using an autosampler and the fluorescence was recorded for 90 minutes per minute with an excitation wavelength of 485 nm and an emission wavelength of 535 nm. The plate was automatically shaken before each reading. A buffer blank (FL + AAPH) instead of antioxidant or Trolox calibration was carried out in each assay. The samples were evaluated at different concentrations (1-10 μM). All the reaction solution was prepared in duplicate, and each sample was tested at least three independent assays. The area under the fluorescence decay curve (AUC) was automatically calculated by the instrument. The blank AUC was subtracted to obtain the net AUC of

the sample. ORAC-FL value of each sample was expressed as Trolox equivalents by using the standard curve where the ORAC-FL value of Trolox was taken as.

4.2.5. Evaluation of metal-chelating activity

The chelating studies were performed using a Varioskan Flash Multimode Reader (Thermo Scientific). After the methanol solution of the tested compound alone or in the presence of $CuCl_2$, $ZnCl_2$, $AlCl_3$, and $FeSO_4$ incubated for 30 min at room temperature, the UV absorption spectra was recorded under wavelength ranging from 200 to 600 nm. The final concentrations of tested compound and metals were 37.5 μM. The difference UV-vis spectra due to complex formation were obtained by numerical subtraction of the spectra of the metal alone and the compound alone from the spectra of the mixture.

Titrating the methanol solution of tested compound with ascending of $CuCl_2$ to get the stoichiometry of the compound-Cu^{2+} complex. The final concentration of tested compound was also 37.5 μM, and the final concentration of $CuCl_2$ ranged from 3.75 to 150 μM. The UV spectra were recorded and treated by numerical subtraction of $CuCl_2$ and tested compound at corresponding concentrations, plotted versus the mole fraction of tested compound.

4.2.6. Evaluation of self- and Cu^{2+}-induced Aβ_{1-42} aggregation inhibitiory activity

The inhibitory activities of compounds on self- and Cu^{2+}-induced Aβ_{1-42} aggregation was performed using a Thioflavin T-based fluorometric assay.[37-40] Thioflavin T (ThT) was purchased from TCI (Shanghai) Development. 1,1,1,3,3,3-hexafluoro-2-propanol (HFIP) was purchased from Energy Chemical. β-Amyloid$_{1-42}$ (Aβ_{1-42}), supplied as trifluoroacetate salt, was purchased from GL Biochem Ltd. Aβ_{1-42} was dissolved in HFIP (1 mg/mL) and incubated for 24 h at room temperature, then the solvent was evaporated at room temperature. The residue was dissolved in dry DMSO to the concentration of 200 μM and kept frozen at –80 °C. The DMSO solution of tested compounds in 2.5 mM were stored and diluted with phosphate buffer solution (pH 7.4) before use.

For the self-induced aggregation assay, 20 μL Aβ_{1-42} (25 μM, final concentration) and 20 μL test compounds (25 μM, final concentration) diluted with 50 mM phosphate buffer solution (pH 7.40) were added and incubated at 37 °C for 24 h. A transparent heat-resistant plastic film was used to seal the plate to minimize evaporation effect. After the incubation, 160 μL of 5 μM ThT in 50 mM glycine-NaOH buffer (pH 8.5) was added. Each assay was carried out in triplicate. Fluorescence was measured on a Varioskan Flash Multimode Reader (Thermo Scientific) with excitation and emission

wavelengths of 446 nm and 490 nm, respectively. Calculate the percent inhibition by the following expression: $(1\text{-}IF_i/IF_c) \times 100$. And IF_i and IF_c are the fluorescence intensities obtained for A$\beta_{1\text{-}42}$ after subtracting the background in the presence and absence of inhibitors, respectively.

For the Cu^{2+}-induced A$\beta_{1\text{-}42}$ aggregation assay, standard solutions of Cu^{2+} was diluted with the HEPES buffer (20 mM, pH 6.60, 150 mM NaCl) to the concentration of 75 μM. The A$\beta_{1\text{-}42}$ stock solution was diluted with HEPES buffer. The mixture of 20 μL A$\beta_{1\text{-}42}$ (25 μM, final concentration) and 20 μL Cu^{2+} (25 μM, final concentration), with or without 20 μL tested compound (25 μM, final concentration) was incubated at 37 °C for 24h. Then, 190 μL of 5 μM ThT in 50 mM glycine-NaOH buffer (pH 8.50) was added. Each assay was run in triplicate. The detection method was the same as above.

4.2.7. Evaluation of effect on the disaggregation of A$\beta_{1\text{-}42}$ aggregation

For the disaggregation of self-induced Aβ fibrils experiment, the A$\beta_{1\text{-}42}$ stock solution was diluted with HEPES buffer (20 mM, pH 6.6, 150 mM NaCl). 20 μL A$\beta_{1\text{-}42}$ (50 mM) was incubated at 37 °C for 24 h. Then 20 μL tested compound (25 mM, final concentration) was added and the mixture was incubated at 37 °C for another 24 h. To reduce the evaporation effect, the plates were sealed by a transparent heat-resistant plastic film. After incubation, 160 mL of 5 mM ThT in 50 mM glycine-NaOH buffer (pH 8.5) was added. Each assay was run in triplicate. The detection method was the same as above.

For the disaggregation of copper-induced Aβ fibrils experiment, the A$\beta_{1\text{-}42}$ stock solution was diluted with HEPES buffer. The mixture of 20 μL A$\beta_{1\text{-}42}$ (25 mM, final concentration) and 20 μL Cu^{2+} (25 mM, final concentration) was incubated 37 °C for 24 h. 20 μL tested compound (25 mM, final concentration) was then added and the mixture was incubated at 37 °C for another 24 h. The plates were sealed by a transparent heat-resistant plastic film to reduce the evaporation effect. After incubation, 190 mL of 5 mM ThT in 50 mM glycine-NaOH buffer (pH 8.5) was added. Each assay was run in triplicate. The detection method was the same as above.

4.2.8. In vitro blood-brain barrier permeation assay

The *in vitro* blood-brain barrier permeation assay was conducted using the artificial membrane permeation assay of the blood-brain barrier (PAMPA-BBB) described by Di *et al*.[42] The acceptor plate (PVDF membrane, pore size 0.45 μm, MAIPN4550) and the donor plate (MATRNPS50) were purchased from Millipore. And porcine brain lipid (PBL) was purchased from Avanti Polar Lipids.

Filter PDVF membrane units (diameter 25 mm, pore size 0.45 μm) were purchased from Pall Corporation. Test compounds were dissolved in DMSO at 5 mg/mL and diluted to a final concentration of 100 μg/mL with PBS/EtOH (70:30). The filter membrane was coated with 4 μL dodecane solution of PBL (20 μg/mL) and 200 μL of PBS/EtOH (70:30) were added to the acceptor wells. Then the donor wells were filled with 350 μL of the compound solutions (100 μg/mL). The acceptor filter plate was carefully placed on the donor plate, and allowed to stand at 25 °C for 18 h. After that, the two plates were separated and the concentrations of drug in the donor and acceptor wells were determined using the Varioskan Flash Multimode Reader (Thermo Scientific). Each sample was analyzed at ten wavelengths in four wells and run at least three times independently. Calculate P_e using the following expression:

$$P_e = -\ln [1 - C_A(t)/C_{equilibrium}]/[A \times (1/V_D + 1/V_A) \times t]$$

$$C_{equilibrium} = [C_D(t) \times V_D + C_A(t) \times V_A]/(V_D + V_A)$$

Wherein P_e is the permeability in cm/s.. $C_A(t)$ is the concentration of the compound in the acceptor well at time t. $C_D(t)$ is the concentration of the compound in the donor well at time t. A is effective filter area and t is the permeation time. V_D is the volume of donor well. V_A is the volume of acceptor well. Results are taken as the mean ± SD. In the experiment, 11 quality control drugs with known BBB permeability were used to verify the validation analysis group.

4.2.9. In vitro anti-inflammatory activity evaluation

The *in vitro* cytotoxicity and inhibition activities of LPS-induced NO and TNF-*α* production were investigated to evaluate the anti-inflammatory activity of these compounds.[43-46] BV-2 cell-line were cultured in Dulbecco's modified eagle medium (DMEM) in a humidified incubator containing 5% CO_2 at 37 °C. DMEM was purchased from Gibco including 2mM glutamine, 10% fetal bovine serum,1 mM pyruvate, streptomycin (10 μg/mL) and penicillin (100 U/mL). All the test compounds in DMSO were diluted with PBS to various concentrations.

The *in vitro* cytotoxicity assay was performed by the MTT method. MTT (3-(4,5-dimethylthiazol-2-yl)-2,5-diphenyltetrazolium bromide) was dissolved in PBS at 5 mg/mL, and the solution was than sterilized and filtered to remove a small amount of insoluble residue. BV-2 cells prepared in DMEM (100 μL) were added to the plates and incubated at 37 °C for 24 h in a humidified incubator with 5% CO_2. Then 10 μL test samples were added to confluent cells in triplicate wells. The plates were incubated for 30 min. After that 10 μL LPS (1.0 μg/mL) was added,

and the treated wells were incubated for another 24 h. Then 100 μL MTT solution was added to each well. The plates were incubated for 4 h. The formed crystals were dissolved in 200 μL DMSO and the absorbance at 490 nm was measured using a spectrophotometer. Results are expressed as percent viability compared to untreated cells.

Inhibition of LPS-induced NO production was measured by using a Griess reaction method. BV-2 cells prepared in DMEM (100 μL) were added to the plates and incubated at 37 °C for 24 h in a humidified incubator with 5% CO_2. $NaNO_2$ was dissolved in the mixed solution of PBS and DMEM and diluted to various concentrations (0, 1.5625, 3.125, 6.25, 12.5, 25, 50 and 100 μM). 10 μL test samples were added to confluent cells in triplicate wells. After that the treated wells were incubated for 30 min. And then 10 μL LPS (1.0 μg/mL) was added, and BV2-cells were stimulated with LPS for 24 h in the presence of test samples. LPS-induced NO production from BV-2 cells was determined by measuring the concentration of $NaNO_2$ in culture supernatant. 50 μL samples of culture media were incubated with 50 μL Griess reagent (1% sulfanilamide, 0.1% naphthylethylene diamine in 2.5% phosphoric acid solution) at room temperature for 10 min. Absorbance at 540 nm was read using an ELISA plate reader. Standard calibration curves of $NaNO_2$ were preparedas standard.

Inhibition of LPS-induced TNF-α production was measured by using an Enzyme-linked immunosorbent assay (ELISA). BV-2 cells prepared in DMEM (100 μL) were cultured in 96-well cell culture microplate and incubated at 37 °C for 24 h in a damp incubator with 5% CO_2. 10 μL test samples were added to confluent cells in triplicate wells. After that, the treated wells were incubated for 30 min. And then 10 μL LPS (1.0 μg/mL) was added, BV2-cells were stimulated with LPS for 24 h in the presence of test samples. The TNF-α released from BV-2 cells was measured by ELISA assay according to the manufacturer's instructions.

Acknowledgments

This work was supported by Sichuan Science and Technology Program (2018SZ0014), the National Science and Technology Major Project on "Key New Drug Creation and Manufacturing Program" (2013ZX09301304-002) and Sichuan Youth Science and Technology Innovation Research Team Funding (2016TD0001).

Appendix A. Supplementary Material

The supplementary data associated with this article can be found in the online version.

References

[1] K. Arora, N. Alfulaij, J.K. Higa, J. Panee, R.A. Nichols, Impact of sustained exposure to β-amyloid on calcium homeostasis and neuronal integrity in modenerve cell system expressing $\alpha_4\beta_2$ nicotinic acetylcholine receptors, Journal of Biological Chemistry, 288 (2013) 11175-11190.

[2] M. A. Daulatzai, Fundamental role of pan-inflammation and oxidative-nitrosative pathways in neuropathogenesis of Alzheimer's disease, American Journal of Neurodegenerative Disease, 5 (2016) 102-130.

[3] T.L. Emmerzaal, A.J. Kiliaan, D.R. Gustafson, 2003-2013: A decade of body mass index, Alzheimer's disease, and dementia, Journal of Alzheimer's Disease, 43(2015) 739-755.

[4] H.W. Querfurth, F.M. Laferla, Alzheimer's disease, New England Journal of Medicine, 362 (2010) 329-344.

[5] S.Y. Hung, W.M. Fu, Drug candidates in clinical trials for Alzheimer's disease, Journal of Biomedical Science, 24 (2017) 47.

[6] S. Kar, S.P. Slowikowski, D. Westaway, H.T. Mount, Interactions between β-amyloid and central cholinergic neurons: implications for Alzheimer's disease，Journal of Psychiatry & Neuroscience, 29 (2004) 427-441.

[7] D. Muñoz-Torrero, P. Camps, Dimeric and hybrid anti-Alzheimer drug candidates, Current Medicinal Chemistry, 13 (2006) 399-422.

[8] D.R. Liston, J.A. Nielsen, A. Villalobos, D. Chapin, S.B. Jones, S.T. Hubbard, I.A. Shalaby, A. Ramirez, D. Nason, W.F. White, Pharmacology of selective acetylcholinesterase inhibitors: implications for use in Alzheimer's disease, European Journal of Pharmacology, 486 (2004) 9-17.

[9] C. Haass, D.J. Selkoe, Soluble protein oligomers in neurodegeneration: lessons from the Alzheimer's amyloid β-peptide, Nature Reviews Molecular Cell Biology, 8 (2007) 101-112.

[10] K. Ubhi, E. Masliah, Alzheimer's disease: recent advances and future perspectives, Journal of

Alzheimer's Disease, 33 (2013) 185-194.

[11] P. Mao, P.H. Reddy, Aging and amyloid beta-induced oxidative DNA damage and mitochondrial dysfunction in Alzheimer's disease: implications for early intervention and therapeutics, Biochimica et Biophysica Acta, 1812 (2011) 1359-1370.

[12] J.S. Aprioku, Pharmacology of free radicals and the impact of reactive oxygen species on the testis, Journal of Reproduction & Infertility, 14 (2013) 158-172.

[13] A. Rampa, F. Belluti, S. Gobbi, A. Bisi, Hybrid-based multitarget ligands for the treatment of Alzheimer's disease, Current Topics in Medicinal Chemistry, 11(2011) 2716-2730.

[14] E. Gaggelli, H. Kozlowski, D. Valensin, G. Valensin, Copper homeostasis and neurodegenerative disorders (Alzheimer's, prion, and Parkinson'sdiseases and amyotrophic lateral sclerosis), Chemical Reviews, 106 (2006) 1995-2044.

[15] G. Halliday, S.R. Robinson, C. Shepherd, J. Kril, Alzheimer’s disease and inflammation: a review of cellular and therapeutic mechanisms, Clinical and Experimental Pharmacology & Physiology, 27 (2000) 1-8.

[16] J.L. Teeling, V.H. Perry, Systemic infection and inflammationin acute CNS injury and chronic neurodegeneration: underlying mechanisms, Neuroscience, 158 (2009) 1062-1073.

[17] J. Hoozemans, R. Veerhuis, J. Rozemuller, P. Eikelenboom, Neuroinflammation and regeneration in the early stages of Alzheimer's disease pathology, International Journal of Developmental Neuroscience, 24 (2006)157-165.

[18] A. Okello, P. Edison, H. Archer, F. Turkheimer, J. Kennedy, R. Bullock, Z. Walker, A. Kennedy, N. Fox, M. Rossor, Microglial activation and amyloid deposition in mild cognitive impairment a PET study, Neurology, 72 (2009) 56-62.

[19] G.P. Lim, F. Yang, T. Chu, P. Chen, W. Beech, B. Teter, T. Tran, O. Ubeda, K.H. Ashe, S.A. Frautschy, G.M. Cole, Ibuprofen suppresses plaque pathology and inflammation in a mouse model for Alzheimer’s disease, Journal of Neuroscience, 20 (2000) 5709-5714.

[20] Y.P. Tang, S.Z. Haslam, S.E. Conrad, C.L. Sisk, Estrogen increasesbrain expression of the mRNA encoding transthyretin, an amyloid beta scavenger protein, Journal of Alzheimer’s Disease, 6 (2004) 413-420.

[21] A. Benvidia，M. Rezaeinasaba，S. Gharaghanib，S. Abbasia，H.R. Zarea，Experimental and theoretical investigation of interaction between bovine serum albumin and the mixture of caffeic

acid and salicylic acid as the antioxidants，Electrochimica Acta, 255 (2017) 428-441.

[22] V.M. Nurchi, M. Crespo-Alonso, L. Toso, J.I. Lachowicz, G. Crisponi, G. Alberti, R. Biesuz, A. Domínguez-Martín, J. Niclós-Gutíerrez, J.M. González-Pérez, M.A. Zoroddu, Iron^{III} and aluminium^{III} complexes with substituted salicylaldehydes and salicylic acids, Journal of Inorganic Biochemistry, 128 (2013) 174-182.

[23] S. Muraoka, T. Miura, Inactivation of cholinesterase induced by non-steroidal anti-inflammatory drugs with horseradish peroxidase: implication for Alzheimer's disease. Life Sciences**,** 84 (2009) 272-277.

[24] X. Qiang, Z. Sang, W. Yuan, Y. Li, Q. Liu, P. Bai, Y. Shi,; W. Ang, Z. Tan, Y. Deng, Design, synthesis and evaluation of genistein-*O*-alkylbenzylamines as potential multifunctional agents for the treatment of Alzheimer's disease, European Journal of Medicinal Chemistry, 76 (2014) 314-331.

[25] A. Cavalli, M.L. Bolognesi, S. Capsoni, V. Andrisano, M. Bartolini, E. Margotti, A. Cattaneo, M. Recanatini, C. Melchiorre, A small molecule targeting the multifactorial nature of Alzheimer's disease, Angewandte Chemie International Edition, 46 (2007) 3689-3692.

[26] C. Lemouchi, C.S. Vogelsberg, L. Zorina, S. Simonov, P. Batail, S. Brown, M.A. Garcia-Garibay, Ultra-fast rotors for molecular machines and functional materials via halogen bonding: crystals of 1,4-bis(iodoethynyl) bicyclo [2.2.2] octane with distinct gigahertz rotation at two sites, Journal of the American Chemical Society,133 (2011) 6371-6379.

[27] L. Hintermann, K. Suzuki, 2,5-Dihydroxyterephthalates, 2,5-dichloro-1,4-benzoquinone-3,6-dicarboxylates and polymorphic 2,5-dichloro-3,6-dihydroxyterephthalates, Synthesis, 14 (2008) 2303-2306.

[28] Q. Liu, X. Qiang, Y. Li, Z. Sang, Y. Li, Z. Tan, Y. Deng, Design, synthesis and evaluation of chromone-2-carboxamido-alkylbenzylamines as multifunctional agents for the treatment of Alzheimer’s disease, Bioorganic & Medicinal Chemistry, 23 (2015) 911-923.

[29] F. Mu, S. L. Coffing, D.J. Riese, R.L. Geahlen, P. Verdier-Pinard, E.Hamel, J. Johnson, M. Cushman, Design, synthesis, and biological evaluation of a series of lavendustin A analogues that inhibit EGFR and syk tyrosine kinases, as well as tubulin polymerization, Journal of Medicinal Chemistry, 44 (2001) 441-452.

[30] Z. Hailin, M. B. H. Youdim, F. Mati, Selective acetylcholinesterase inhibitor activated by

acetylcholinesterase releases an active chelator with neurorescuing and anti-amyloid activities, ACS Chemical Neuroscience, 1(2010) 737-746.

[31] C. Lu, Q. Zhou, J. Yan, Z. Du, L. Huang, X. Li, A novel series of tacrine-selegiline hybrids with cholinesterase and monoamine oxidase inhibition activities for the treatment of Alzheimer's disease, European Journal of Medicinal Chemistry, 62 (3013) 745-753.

[32] Y. He, P. F. Yao, S. B. Chen, Z. H. Huang, S. L. Huang,; J. H. Tan, D. Li, L. Q. Gu, Z. S. Huang, Synthesis and evaluation of 7,8-dehydrorutaecarpine derivatives as potential multifunctional agents for the treatment of Alzheimer's disease, European Journal of Medicinal Chemistry, 63C (2013) 299-312.

[33] Y. Bourne, J. Grassi, P. E. Bougis, P. Marchot, Conformational flexibility of the acetylcholinesterase tetramer suggested by X-ray Crystallography, The Journal of Biological Chemistry, 274 (1999) 30370-30376.

[34] A. Dávalos, C. Gómez-Cordovés, B. Bartolomé, Extending applicability of the oxygen radical absorbance capacity (ORAC-fluorescein) assay, Journal of Agricultural and Food Chemistry, 52 (2004) 48-54.

[35] Y. Li, X. Qiang, L. Luo, Y. Li, G. Xiao, Z. Tan, Y. Deng, Synthesis and evaluation of 4-hydroxyl aurone derivatives as multifunctional agents for the treatment of Alzheimer's disease, Bioorganic & Medicinal Chemistry, 24 (2016) 2342-2351.

[36] L. Huang, C. Lu, Y. Sun, F. Mao, Z. Luo, T. Su, H. Jiang, W. Shan, X. Li, Multitarget-directed benzylideneindanone derivatives: anti-*β*-amyloid (A*β*) aggregation, antioxidant, metal chelation, and monoamine oxidase B (MAO-B) inhibition properties against Alzheimer’s disease, Journal of Medicinal Chemistry, 55 (2012) 8483-8492.

[37] N. García-Font, H. Hayour, A. Belfaitah, J. Pedraz, I. Moraleda, I. Iriepa, A. Bouraiou, M. Chioua, J. Marco-Contelles, M. J. Oset-Gasque, Potent anticholinesterasic and neuroprotective pyranotacrines as inhibitors of beta-amyloid aggregation, oxidative stress and tau-phosphorylation for Alzheimer's disease, European Journal of Medicinal Chemistry, 118 (2016) 178-192.

[38] Z. Sang, X. Qiang, Y. Li, W. Yuan, Q. Liu, Y. Shi, W. Ang, Y. Luo, Z. Tan, Y. Deng, Design, synthesis and evaluation of scutellarein-*O*-alkylamines as multifunctional agents for the treatment of Alzheimer's disease, European Journal of Medicinal Chemistry, 94 (2015) 348-366.

[39] M. Chioua, J. Pérez-Peña, N. García-Font, I. Moraleda, I. Iriepa, E. Soriano, J. Marco-Contelles, M.J. Oset-Gasque, Pyranopyrazolotacrines as nonneurotoxic, Aβ-anti-aggregating and neuroprotective agents for Alzheimer's disease, Future Medicinal Chemistry, 7 (2015) 845-855.

[40] M. Bartolini, C. Bertucci,; M.L. Bolognesi, A. Cavalli, C. Melchiorre, V. Andrisano, Insight into the kinetic of amyloid β (1-42) peptide self-aggregation: elucidation of inhibitors mechanism of action. ChemBioChem, 8 (2007) 2152-2161.

[41] Z. Sang, X. Qiang, Y. Li, R. Xu, Z. Cao, Q. Song, T. Wang, X. Zhang, H. Liu, Z. Tan, Y. Deng, Design, synthesis and evaluation of scutellarein-O-acetamido alkylbenzylamines as potential multifunctional agents for the treatment of Alzheimer's disease, European Journal of Medicinal Chemistry, 135 (2017) 307-323.

[41] L. Di, E.H. Kerns, K. Fan, O.J. McConnell, G.T. Carter, High throughput artificial membrane permeability assay for blood-brain barrier, European Journal of Medicinal Chemistry, 38 (2003) 223-232.

[43] Z. Cao, J. Yang, R. Xu, Q. Song, X. Zhang, H. Liu, X. Qiang, Y. Li, Z. Tan, Y. Deng, Design, synthesis and evaluation of 4'-OH-flurbiprofen-chalcone hybrids as potential multifunctional agents for Alzheimer's disease treatment, Bioorganic & Medicinal Chemistry, 26 (2018) 1102-1115.

[44] J.Y. Kim, H. J. Lim, J. S. Kim, D. H. Kim, H. J. Lee, H. D. Kim, R. Jeon, J.H. Ryu, In vitro anti-inflammatory activity of lignans isolated from magnolia fargesii, Bioorganic & Medicinal Chemistry Letters, 19 (2009) 937-940.

[45] Y.X. Yang, L.T. Zheng, J.J. Shi, B. Gao, Y.K. Chen, H.C. Yang, H.L. Chen, Y.C. Li, X.C. Zhen, Synthesis of 5α-cholestan-6-one derivatives and their inhibitory activities of NO production in activated microglia: discovery of a novel neuroinflammation inhibitor, Bioorganic & Medicinal Chemistry Letters, 24 (2014) 1222-1227.

[46] G.K. Hagos, S.O. Abdul-Hay, J. Sohn, P.D. Edirisinghe, R.E.P. Chandrasena, Z. Wang, Q. Li, G.R. Thatcher, Anti-inflammatory, antiproliferative, and cytoprotective activity of NO chimera nitrates of use in cancer chemoprevention, Molecular Pharmacology, 74 (2008) 1381-1391.

Graphical abstract